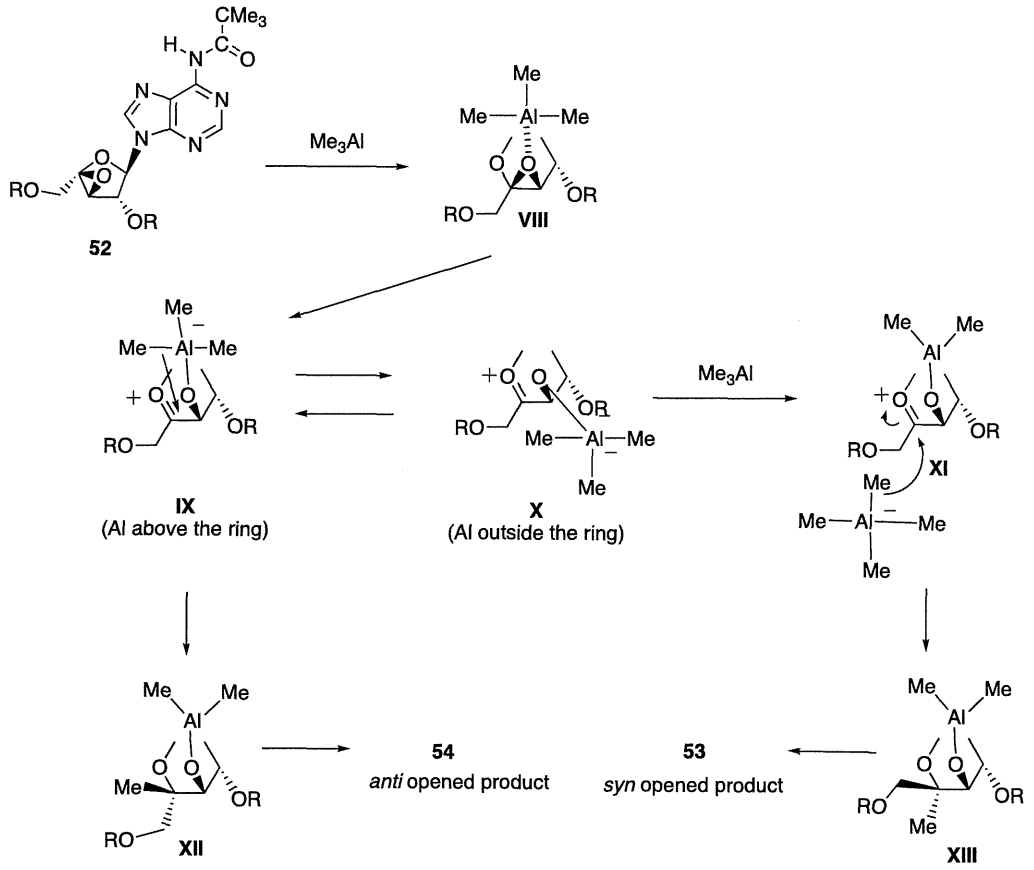

Scheme 19. Proposed Reaction Mechanism for the Ring Opening of Epoxide **52**.

other conformer **XI**, it is outside the ring avoiding either steric or electronic repulsion with the adenine base.

When the amount of the remaining Me_3Al is limited or it is complexed with an ethereal solvent, intramolecular attack of the methyl ligand from **IX** would be inevitably take place to give **XII** (*syn*-opening), which is finally converted to **53**. On the other hand, in the case of where non-coordinated Me_3Al is sufficiently available in CH_2Cl_2, there is a good opportunity for **X** to transfer its methyl ligand to Me_3Al, yielding tetramethylaluminate and **XI**. Under such circumstances, the presence of the adenine base as well as the 3′-alkoxyaluminum substituent in **XI** would render the stereochemical bias in favor of less hindered attack to lead to the dominant formation of **XIII** (*anti*-opening), which gives **54** after workup.

Such transfer of the methyl ligand from **X** to Me_3Al would also be affected by the concentration of Me_3Al in the reaction medium. In fact, when the reaction was carried out in a 50-fold diluted medium, the ratio of **53/54** was changed from 5/1 to 1.5/1.

One would imagine that the stereochemical outcome of this reaction also would be affected by the bulkiness of the 2′-*O*-silyl group. The ratio of **53/54** = 5/1 observed for **51** became 10/1 when the corresponding TES (triethylsilyl)-protected epoxide was employed (Scheme **20** and Table **2**). It was beyond our expectation that the TBDPS (di-*tert*-butyldiphenylsilyl)-protected epoxide **61** gave the reverse stereoselectivity (**62/63** = 1/7).

A significant change of the ratio was also observed by varying the reaction temperature. At a higher temperature, almost equal amounts of **53** and **54** were formed (at 0 °C, 1.4/1; at room temperature, 0.7/1). At a lower temperature of –80 °C, the ratio was inverted and became 30/1. By combining the experimental results obtained thus far, the highest stereoselectivity (**53/54** = 50/1, combined yield 90%) was attained by carrying out the reaction at –80 °C in CH_2Cl_2 employing the TES protected epoxide (Scheme **21**).

(5) Ring opening of 4′,5′-epoxy thymine nucleosides: finding of a promising anti-HIV-1 agent 4′-ethynylstavudine

This study was motivated by fairly recent reports that 4′-substituted nucleosides show significant inhibitory activity against HIV proliferation [24-29]. Since the most commonly utilized method for the synthesis of these compounds is manipulation of 4′-hydroxymethyl derivatives of nucleosides or sugars prepared via aldol-Cannizzaro reaction [30-31], we intended to develop a new and general method based on nucleophilic ring opening of a suitable 4′,5′-epoxy structure.

Ring opening of the epoxide **65** prepared from 4′,5′-unsaturated thymidine derivative **64** was first examined using Me_3Al (Scheme **22**) [32]. As a result, dominant formation of the 4′-methyl-α-L-isomer **67** was observed, the desired β-D-isomer **66** being formed only in 5% yield. This unsatisfactory outcome is assumed to be due to conformational preference of the oxonium intermediate depicted as **XV**, which can avoid the steric repulsion between the 5′-*O*-aluminate and the 3′-*O*-TBDMS group. In fact, the 4′,5′-epoxide **68** having the opposite 3′-configuration to **65** (Scheme **23**), upon reacting with Me_3Al, gave solely the 4′-methyl-β-D-isomer **69** (72%) through the aluminate **XXVI**. By applying this method, the 4′-vinyl **70** and 4′-ethynyl **71** derivatives also were prepared. This method was found to be applicable to the respective purine nucleosides.

To effect inversion at the 3′-position of these 4′-branched products by nucleophilic substitution, 4′-methyl derivative **69** was converted into chloromesyl nucleoside **73** following 2 steps (Scheme **24**). When **73** was reacted with cesium acetate in the pres-

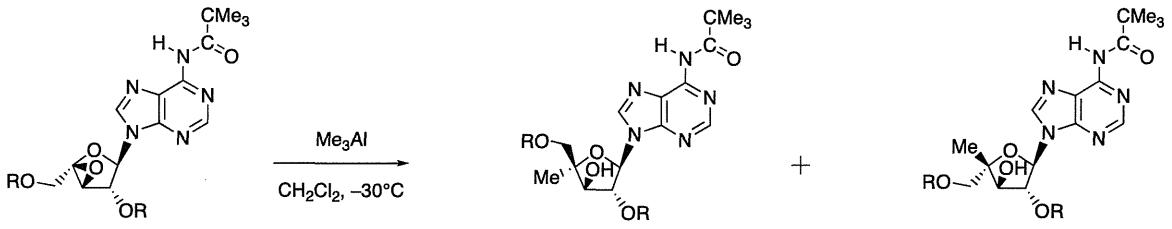

52: R = TBDMS
58: R = $SiEt_3$
61: R = TBDPS
TBDPS : *t*-butyldiphenylsilyl

53: R = TBDMS
59: R = $SiEt_3$
62: R = TBDPS

54: R = TBDMS
60: R = $SiEt_3$
63: R = TBDPS

Scheme 20. Effect of Bulkiness of the Protecting Group for the ratio of *Anti*-Opened/*Syn*-Opened Products.

Table 2. Reaction of **52**, **58** and **61** with Me_3Al

entry	epoxide	products	combined yield (%) of the two isomers	ratio of β-D-isomer/α-L-isomer
1	**52**	**53** and **54**	90	**53** and **54** = 5/1
2	**58**	**59** and **60**	89	**59** and **60** = 10/1
3	**61**	**62** and **63**	94	**62** and **63** = 1/7

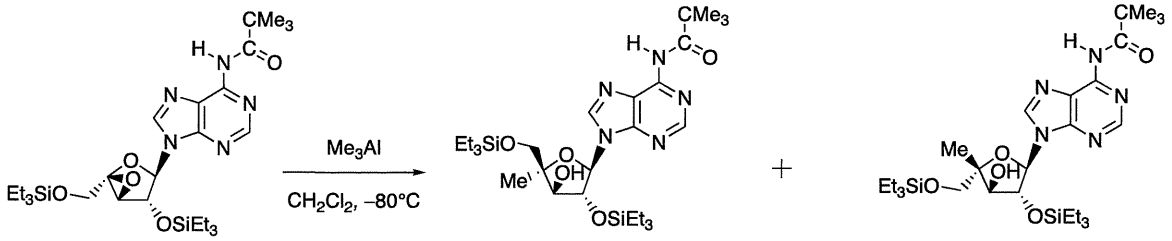

58

59

60

Scheme 21. Optomized Reaction Conditions leading to *Anti*-Opened Product **59.**

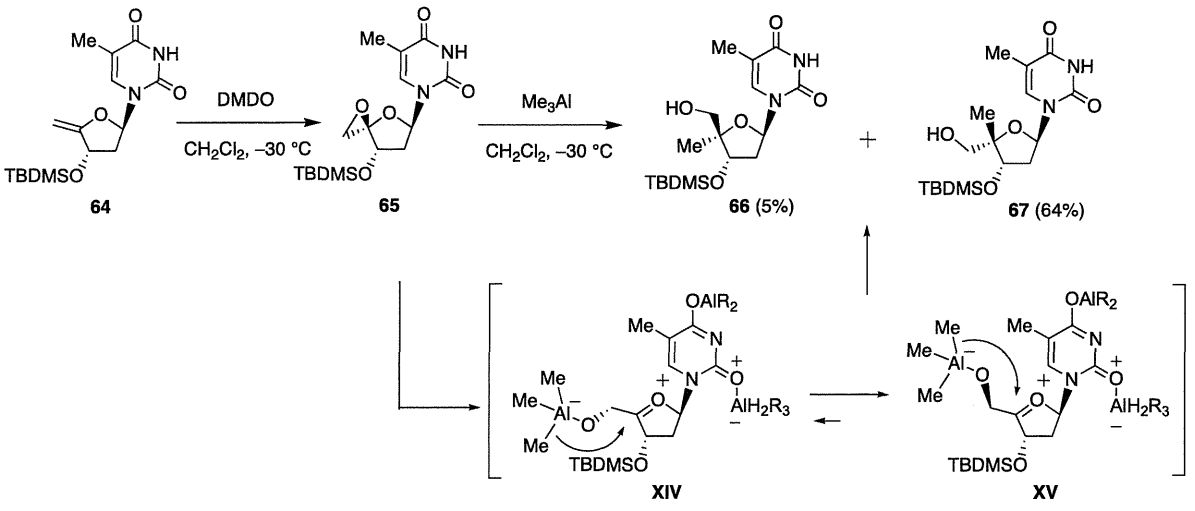

64

65

66 (5%)

67 (64%)

Scheme 22. Epoxidation of 4',5'-Unsaturated thymidine **64** and Ring Opening of 4',5'-Epoxide **65** with Me_3Al.

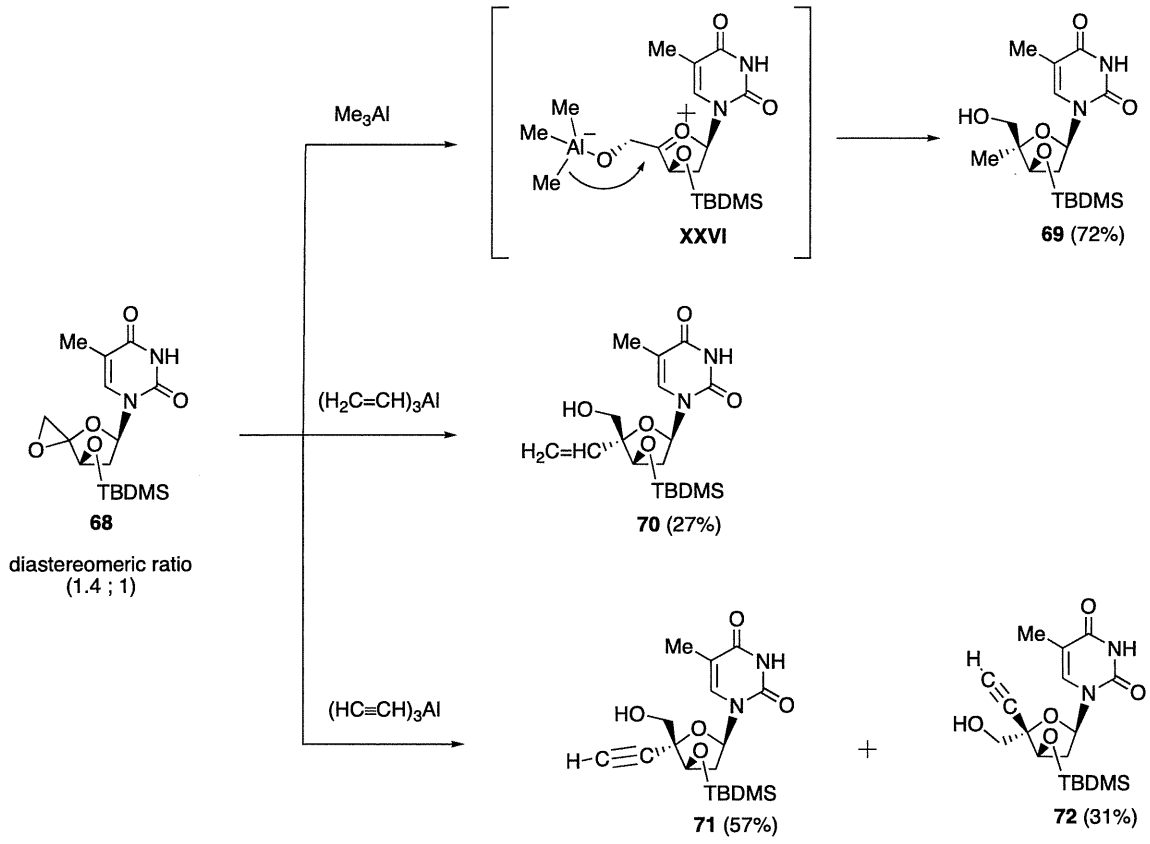

Scheme 23. Ring Opening of 4',5'-Epoxythymine Nucleoside **68** with Organoaluminum Reagents.

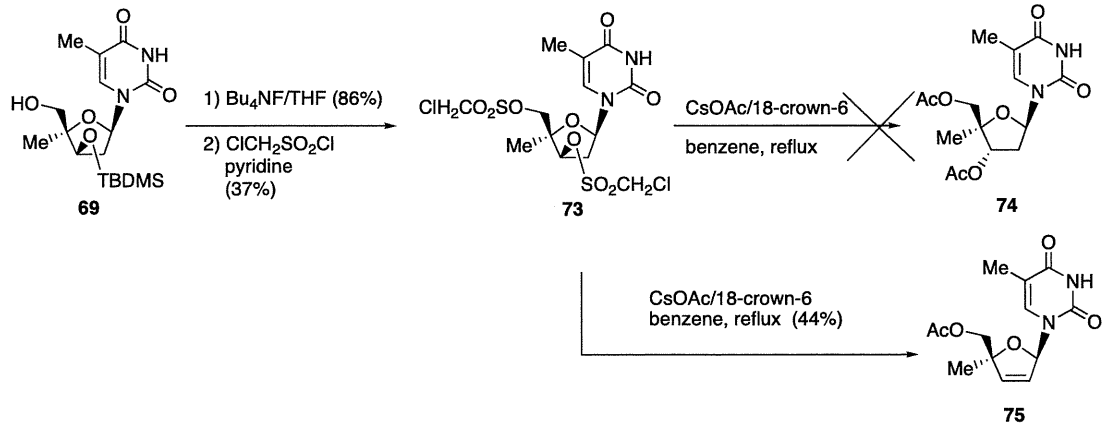

Scheme 24. Attemtps to Effect Inversion at the 3'-Position of **69** and Formation of Elimination Products **75.**

ence of 18-crown-6 in benzene under reflux conditions, the expected thymidine derivative **74** could not be obtained but the eliminated 4'-methyl d4T **75** was formed. The obtained nucleoside is 4'-methyl derivative of clinically used anti-HIV agent d4T (stavudine). Therefore, these 4'-branched products **69-71** were transformed into the respective d4T derivatives (Scheme **25**).

Among these elimination products, 2',3'-didehydro-3'-deoxy-4'-ethynylthymidine (**78**, Ed4T) was found to be more inhibitory against HIV-1 than the parent compound d4T, and much less toxic to various cells and also to mitochondrial DNA synthesis (Table **3**) [33]. This compound has several additional advantages as a promising anti-HIV-1 agent: 1) it is a better substrate for human thymidine kinase than stavudine [34], 2) it is very much more resistant to catabolism by thymidine phosphorylase [34], and 3) its anti-HIV activity is enhanced in the presence of a major mutation K103N [35], associated with resistance non-nucleoside reverse transcriptase inhibitors.

Some structure-activity relationship studies of Ed4T (**78**) also were carried out. For the analogues of **78** to be inhibitory against HIV-1, their 4'-carbon-substituent has to be sp-hybridized like ethynyl and cyano group [36]. Since methylethynyl nucleoside **79** decreased the activity [37], smaller size could be an additional requirement for the 4'-substituent. Although its carbocyclic analogue

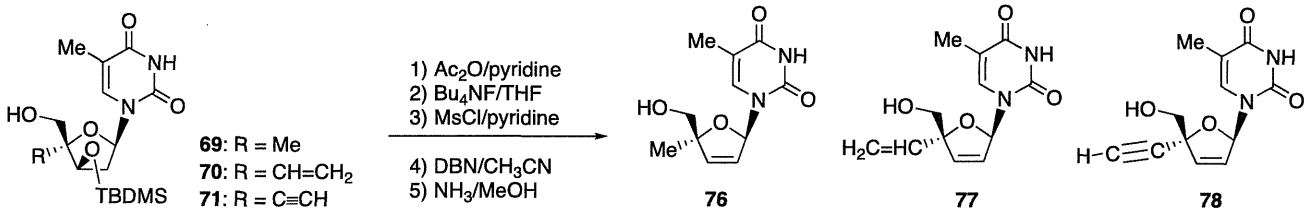

Scheme 25. Synthesis of 4'-Substituted d4T **76-78.**

Table 3. Anti-HIV-1_{IIIB} activity of 4'-carbon-substituted stavudine 76-78[a]

Table 3. Anti-HIV-1_{IIIB} activity of 4'-carbon-substituted stavudine **76-78** [a]

Compd	IC_{50} (μM)[a]	IC_{50} (μM)[b]
76	> 100	> 100
77	> 100	> 100
78 (4'-ethynylstavudine)	0.20	> 100
stavudine	2.8	100

[a] Data taken from ref. 33.
[b] Inhibitory concentration required to achieve 50% protection of MT-2 cells against the cytopathic effect of HIV-1 III_B.
[c] Cytotoxic concentration required to reduce the viability of mock-infected MT-2 cells by 50%.

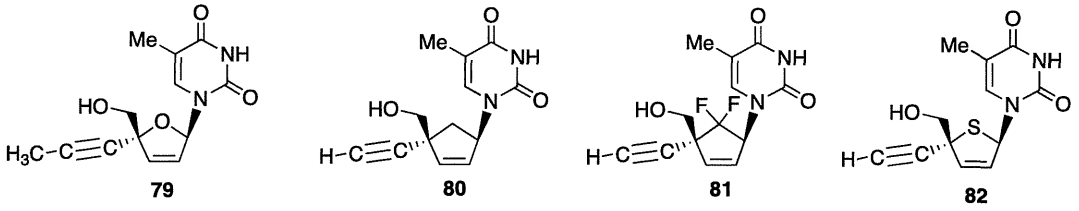

Fig. (6). Structures of Ed4T analogs **79-82.**

80 and **81** resulted in total loss of the activity [38-39], the 4'-thio derivative **82** retains the activity (Fig. (**6**)) [40].

(II) ANTIVIRAL ACTIVITY OF 4'-ETHYNYLSTAVUDINE

The inhibitory effects of 4'-ethynylstavudine, stavudine, and lamivudine on HIV-1 (III_B) replication have been evaluated in MT-2 and MT-4 cells. 4'-Ethynylstavudine exhibited higher activity than satavudine and lamivudine (Table **4**). The 50% effective concentrations (EC_{50}s) of 4'-ethynylstavudine were 0.25 and 0.07 μM in MT-2 cells and MT-4 cells, respectively. The activity of 4'-ethynylstavudine was 5.2-fold higher than that of d4T in MT-2 cells. The compound was 4.4- and 8.5-fold more potent inhibitor of HIV-1 replication in MT-4 cells than d4T and 3TC, respectively. Furthermore, 4'-ethynylstavudine was found to be active against both X4 (III_B) and R5 (Ba-L) strains in peripheral blood mononuclear cells (PBMCs). On the other hand, cytotoxicity of 4'-ethynylstavudine appeared to be lower than that of d4T.

The anti-HIV-1 activity of 4'-ethynylstavudine against various nucleoside reverse transcriptase inhibitor (NRTI)-resistant mutants has been evaluated (Tables **5** and **6**). A012D contains four NRTI-associated mutations (NAMs) (D67K, K70R, T215F and K219Q), which confer a high level (210-fold) resistance to zidovudine [41]. The M184V mutation in reverse transcriptase (RT) also confers a high level resistance to lamivudine [42]. 4'-ethynylstavudine was 6.7-, 10-, and 2.9-fold less active against A012D and the M184V mutants of HXB-2 and NL4-3 compared to the wild-type, respectively (Table **5**). The K65R mutation confers resistance to tenofovir and some NRTIs [43-45] and, the Q151M complex (A62V, V75I, F77L, F116Y, and Q151M) confers resistance to most of the clinically approved NRTIs [46]. While zidovudine, stavudine, didanosine, and lamivudine were 440-, 8.4-, 14- and 2.8-fold less active against the Q15M mutant of HXB-2, respectively, 4'-ethynylstavudine retained potent anti-HIV-1 activity against the mutants harboring the Q151M or K65R mutation (Table **5**). The K103N mutation confers a high level resistance to non-nucleoside reverse transcriptase inhibitors (NNRTIs). In fact, nevirapine (NVP) was 55- and 70-fold less active against the K103N mutants of HXB-2 and NL4-3, respectively (Table **5**). Interestingly, these mutants proved more susceptible to 4'-ethynylstavudine. Furthermore, 4'-ethynylstavudine exhibited its anti-HIV-1 activity against the KK strain, a clinical isolate from a treatment-naive patient, with an EC_{50} of 0.020 μM (Table **6**). Although the activity of 4'-ethynylstavudine was 4.4 to 17.5-fold weaker against clinical isolates (HKW, HNK, HTN, and HTK) harboring multidrug-resistant mutations than that against the KK strain, the compound still retained considerable anti-HIV-1 activity against these mutants.

Table 4. Anti-HIV-1 activity of 4′-ethynylstavudine[a]

Compound	Virus	Cells	EC_{50}[b] (μM)	CC_{50}[c] (μM)
4′-Ed4T	III_B	MT-2	0.25 ± 0.14	> 100
		MT-4	0.07 ± 0.041	> 100
		PBMC	0.0019 ± 0.0002	56 ± 3
	Ba-L	PBMC	0.0076 ± 0.0013	
d4T	III_B	MT-2	1.3 ± 0.4	98 ± 11
		MT-4	0.31 ± 0.07	79 ± 19
		PBMC	0.019 ± 0.004	28 ± 7
	Ba-L	PBMC	0.047 ± 0.027	
3TC	III_B	MT-4	0.60 ± 0.03	> 100

[a]Data from reference 34 and 35
[b]50% Effective concentration
[c]50% Cytotoxic concentration

Table 5. Anti-HIV-1 activity of selected RT inhibitors against various drug-resistant mutants in MAGI-CCR5 cells[a]

Virus	Mutation	EC_{50} (μM)[b]					
		4′-Ed4T	AZT	D4T	ddI	3TC	NVP
A012B	Wild type	0.49 ± 0.05 (1)	0.037 ± 0.003 (1)	0.33 ± 0.17 (1)	1.1 ± 0.2 (1)	0.27 ± 0.06 (1)	ND[c]
A012D	NAMs[d]	3.3 ± 1.2 (6.7)	7.7 ± 1.8 (210)	0.59 ± 0.03 (1.8)	3.6 ± 2.2 (3.3)	1.1 ± 0.4 (3.3)	ND
HXB-2	Wild type	1.5 ± 0.2 (1)	0.17 ± 0.06 (1)	7.6 ± 3.2 (1)	3.8 ± 0.8 (1)	1 ± 0.3 (1)	0.022 ± 0.012
	K65R	1.3 ± 0.3 (0.87)	0.085 ± 0.008 (0.50)	7.8 ± 1.1 (1.1)	10 ± 1 (2.6)	4.7 ± 1.3 (2.6)	ND
	K103N	0.46 ± 0.28 (0.31)	ND	1.2 ± 0.5 (0.16)	ND	ND	1.2 ± 0.5 (55)
	Y181C	1.5 ± 0.5 (1)	ND	5.2 ± 1.3 (0.68)	ND	ND	3.8 ± 0.5 (170)
	M184V	17 ± 2 (10)	0.13 ± 0.02 (0.76)	5.6 ± 0.4 (0.74)	3.7 ± 0.5 (0.97)	> 100* (> 100)	ND
	MDR[e]	1.1 ± 0.3 (0.73)	74 ± 29 (440)	64 ± 8 (8.4)	52 ± 13 (14)	2.8 ± 0.5 (2.8)	ND
NL4-3	Wild type	0.27 ± 0.11 (1)	ND	0.25 ± 0.05 (1)	ND	0.21 ± 0.08 (1)	0.061 ± 0.012 (1)
	K103N	0.16 ± 0.08 (0.59)	ND	0.21 ± 0.04 (0.8)	ND	0.23 ± 0.14 (1)	4.3 ± 0.4 (70)
	M184V	0.79 ± 0.15 (2.9)	ND	0.22 ± 0.07 (0.88)	ND	> 100 (> 476.2)	0.066 ± 0.025 (1)
	K103N + M184V	0.31 ± 0.12 (1.1)	ND	0.2 ± 0.05 (0.8)	ND	> 100 (> 476.2)	2.3 ± 0.4 (37)

[a]Data from reference 35.
[b]All data represent means ± SD for three or four separate experiments. Values in parentheses represent fold increase (a ratio of EC_{50} for wild type to EC_{50} for mutant).
[c]ND, not determined.
[d]Multidrug resistance: NRTI-associated mutations D67N, K70R, T215F, and K219Q
[e]Multidrug resistance: Q151M complex (A62V, V75I, F77L, F116Y, and Q151M)

Table 6. Anti-HIV-1 activity of 4′-Ed4T against multidrug-resistant clinical isolates in PBMCs[a, b]

Virus	Tropism	EC_{50} (μM)	Mutations associated with NRTI resistance[c]
KK	R5	0.020 ± 0.008	Isolated from a treatment-naive patient
HKW	R5	0.35 ± 0.02	M41L, V75L, D67N, M184I, T215Y, K219R
HNK	R5	0.089 ± 0.052	D67N, T69D, K70R, M184V, T215F, K219D
HTN	R5	0.27 ± 0.15	M41L, M184I, T215Y, K219R
HTK	X4	0.15 ± 0.08	M41L, L74V, M184V, T215Y

[a]Data from reference 35.
[b]Except for HKW, all data represent means ± SD for three or four separate experiments. For HKW, the EC_{50} represents the mean ±range for two separate experiments.
[c]Mutations of HKW, HTK, HTN, and HNK were determined by Oka *et al.* (unpublished data).

To examine the emergence of resistance to 4′-ethynylstavudine, repeated passages of HIV-1 (III_B)-infected MT-4 cells in the presence of escalating concentrations of the compound were conducted. Lamivudine induced a virus harboring the M184V mutation on day 29 ($3TC_{29D}$), and the mutant was completely resistant to lamivudine (Table **7**). However, 4′-ethynylstavudine was found to be only 2-fold less active against this mutant. 4′-ethynylstavudine also induced a virus harboring the M184V mutation on day 26 (4′-$Ed4T_{26D}$), which was 1.7-fold less susceptible to the compound. 4′-Ed4T induced a resistant virus harboring three mutations (P119S, T165A, and M184V) on day 81 (4′-ethynylstavudine$_{81D}$), yet 4′-ethynylstavudine still retained sufficient anti-HIV-1 activity against this mutant. We have previously reported that the EC_{50} of 4′-ethynylstavudine against 4′-ethynylstavudine$_{81D}$ was 13 μM, which was 130-fold resistant in comparison to the wild type III_B [35]. Our recent experiment revealed that the EC_{50} against this strain was 2.3 μM (only 10-fold reduction in comparison to the wild type). The resistant virus 4′-ethynylstavudine$_{81D}$ had synonymous mutations at the codons correspond to the amino acid residues E40 and N136 (Table **8**). It was reported that mutations in the connection domain of RT confers drug-resistance [47,48]. Among the mutations, N348I and A360V in the connection domain contribute to increasing resistance to zidovudine [49,50]. The N348I mutation was reported to be highly correlated with the M184V/I mutation [50]. The N348I and A360V mutations confer resistance to zidovudine by increasing excision of incorporated zidovudine through RNase H-dependent and independent mechanism [51]. However, the resistant virus 4′-ethynylstavudine$_{81D}$ did not contain any mutations at the thumb/connection/RNase H domain of RT (Fig. (**7**)).

(III) BIOLOGY AND PHARMACOLOGY OF 4′-ETHYNYLSTAVUDINE

The finding of potent anti-HIV activity of 4′-ethynylstavudine without much impact on mitochondrial DNA (mt-DNA) concentration in drug treated cells indicated that this compound may have less toxicity than stavudine. Since this discovery, a lot of studies have been done to understand the biology and pharmacology of 4′-ethynylstavudine. In summary, 4′-ethynylstavudine promises to be an ideal nucleoside analog with higher potency and therapeutic index, longer half-life of active metabolites in cells, effective against multidrug resistance (MDR) HIV, and high genetic barrier to the development of resistance probably due to the interaction of the compound with HIV reverse transcriptase (RT) [33,34].

Among 4′-substituted compounds synthesized [34], 4′-ethynylstavudine had a higher anti-HIV activity than stavudine, the parent compound) and much less inhibitory activity against cell growth or mt-DNA than either stavudine or zidovidine [34]. The adverse effects of nucleoside analogs are mediated by their effects on host DNA polymerase activity. Mitochondrial DNA polymerase-γ, unlike nuclear DNA (n-DNA) polym- erases, lacks the ability to effectively discriminate against some nucleoside analogs in favor of endogenous nucleic acids [52]. Nucleoside analog-induced inhibition of mt-DNA synthesis is proposed to induce depletion of cellu-

Table 7. Anti-HIV-1 activity of 4′-Ed4T against wild-type and drug-resistant mutants[a]

Strain	EC_{50} (μM)[b]					
	4′-Ed4T			3TC		
III_B (wild type)	0.22	±	0.13	2	±	0.8
	(1)					
III_B ($3TC_{29D}$)	0.41	±	0.08	> 20		
	(1.8)					
III_B (4′-$Ed4T_{26D}$)	0.39	±	0.13	> 20		
	(1.7)					
III_B (4′-$Ed4T_{81D}$)	2.3	±	1.4	> 20		
	(10)					
CC_{50} (μM)[c]	> 20			> 20		

[a]All data represent means ± standard deviations for three separate experiments
[b]EC_{50}: 50% effective concentration based on the inhibition of virus-induced cytopathicity in MT-4 cells
[c]CC_{50}: 50% cytotoxic concentration based on the reduction of viable cell number in mock-infected MT-4 cells

Table 8. Sequence analysis for the RT region of HIV-1 resistant to 4′-Ed4T

Strain		Number of amino acid residue				
		40	119	136	165	184
III_B (wild type)	nucleotide	GAA	CCC	AAC	ACA	ATG
	amino acid	E	P	N	T	M
III_B (4′-$Ed4T_{81D}$)	nucleotide	GG<u>G</u>	<u>T</u>CC	AA<u>T</u>	<u>G</u>CA	<u>G</u>TG
	amino acid	E	<u>S</u>	N	<u>A</u>	<u>V</u>
III_B ($3TC_{29D}$)	nucleotide	GGA	CCC	AAC	ACA	<u>G</u>TG
	amino acid	E	P	N	T	<u>V</u>

The mutated nucleotides or amino acids are indicated with underlines

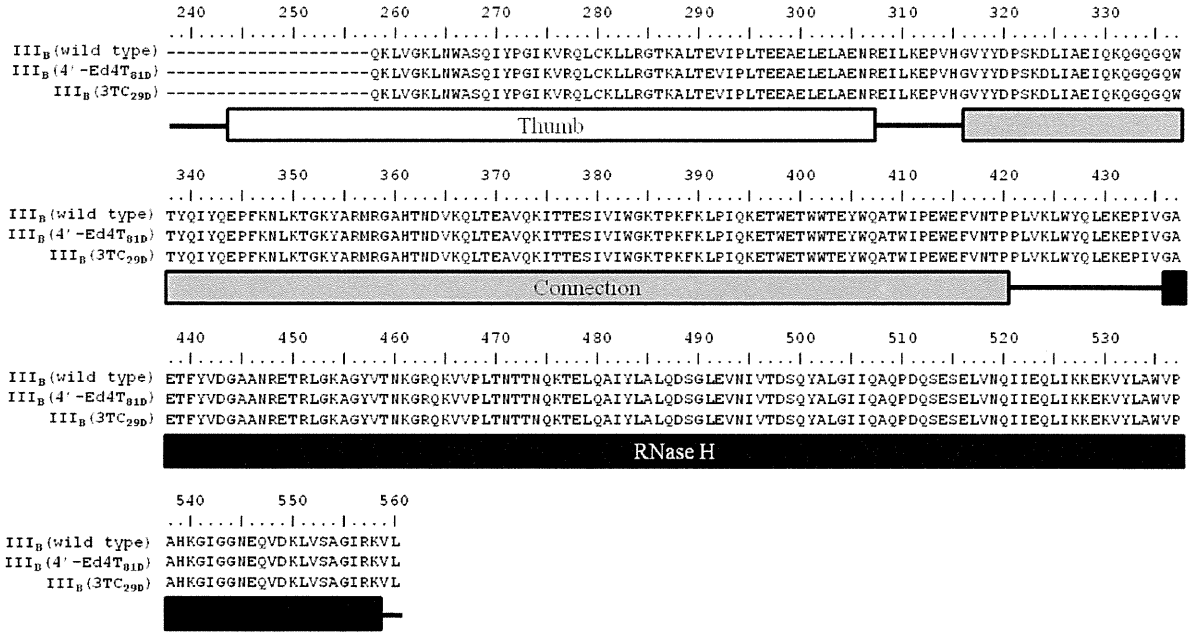

Fig. (7). Sequence Analysis for the Thumb/Connection/RNase H Domain of HIV-1 Resistant to 4′-Ed4T.

lar mt-DNA and is ultimately responsible for the delayed toxicity [53,54]. Both zidovudine and stavudine (stavudine>>zidovudine) cause delayed toxicity in HIV-1 patients due to their impact on mt-DNA and/or n-DNA of affected organs. Interestingly, the IC_{50} values for 4′-Ed4TTP to inhibit pol γ and pol β were both at least 100-fold greater than that for d4TTP (Table **9**) [55]. This is consistent with the observation that 4′-ethynylstavudine caused much less cellular toxicity and mitochondrial DNA less than stavudine in cell culture studies [34]. The underlying molecular mechanism of less inhibition of 4′-Ed4TTP to pol γ and pol β than d4TTP could be due to subtle differences in the interaction of the 4′-position of these two compounds at the active site of at pol γ and pol β.

Table 9. Action of 4′-Ed4TTP on major human DNA polymerases

DNA Polymerase	IC_{50} (μM)[a,b]			
	4′-Ed4TTP	D4TTP	ddTTP	Aphidicolin
α	>100	>100	ND[c]	5
β	>100	1	0.3	ND
γ	~100	1	1	ND
δ	60	40	>100	ND
δ	>100	>100	ND	5

[a] The IC_{50} values represent means from at least three independent experiments with standard deviation less than 20%.
[b] When 0.3μM dTTP was used in the assays.
[c] ND, not determined.

The anti-HIV potency of 4′-ethynylstavudine has been explained by its binding to HIV RT. In steady-state enzymatic analyses, 4′-ethynylstavudine triphosphate (4′-Ed4TTP) inhibited the DNA polymerase activity of RT more efficiently than d4T triphosphate (d4TTP), and the inhibition was more effective on DNA replication with RNA template than with DNA template [55]. 4′-Ed4TTP had much lower *Ki* value in inhibition of RT compared with that for d4TTP also the efficiency of 4′-Ed4TMP incorporation by RT with DNA/RNA substrate was 3-fold lower than that of d4TMP incorporation. The difference between the inhibition and incorporation efficiencies of 4′-Ed4TTP implies that the binding of 4′-Ed4TTP to RT-P/T complex is a more important factor than actual 4′-Ed4TTP incorporation. Moreover, pre-steady-state kinetic studies and computer modeling have illustrated that 4′-Ed4TTP was a better RT inhibitor than d4TTP due to the additional binding of the 4′-ethynyl group at a presumed hydrophobic pocket in the RT active site, which is critical for HIV RT activity (Table **10**) [56]. This hydrophobic pocket is formed by the side chains of A114, Y115, M184, F160 and D185 [52]. These residues are highly conserved, and mutations at this pocket (A114M, A114L, Y115Q, F160A, F160L, and M184F) except M184V and M184A caused complete loss of RT activity [56,57]. M184V could affect the binding of incoming dNTP due to a gap created between the polymerase and the DNA minor groove of the nascent base pair leading to 3 to 5-fold resistance to 4′-Ed4T.

The sine qua non of HIV treatment since 1996 is combination of highly active antiretroviral drugs. When these drugs are used in combination, lower doses may achieve desired antiviral effect with less toxicity. In pre-clinical studies, 4′-ethynylstavudine had synergistic interactions with lamivudine and LFd4C against HIV and was additive in combination with didanosine or zidovudine [34]. Therefore, 4′-ethynylstavudine could be given in combination with several approved antiretroviral drugs in the clinic. 4′-ethynylstavudine is a thymidine analog in the same class as zidovudine and stavudine. However, the phosphorylation of 4′-ethynylstavudine by TK-1 is an essential step but may not be sufficient to explain its potent antiviral activity over stavudine. Since its antiviral effect could be neutralized by dThd but not by dCyd, 4′-ethynylstavudine (like stavudine) acts as a dThd analog; however, the antiviral mechanism of action of 4′-ethynylstavudine could still be quite different from that of stavudine. Stavudine could be more efficiently phosphorylated (using a CEM cellular extract supplemented with partially purified TK-1 and recombinant human dTMP kinase) to the triphosphate metabolite than 4′-ethynylstavudine. This raises

Table 10. Pre-steady-state kinetic parameters for dTMP, d4TMP, and 4′-Ed4TMP incorporation by wt RT and the M184V mutant with DNA/DNA and DNA/RNA P/Ts

P/T	Enzyme	dTTP			d4TTP				4′-Ed4TTP			
		K_d(μM)	K_{pol}(s^{-1})	K_{pol}/K_d ($\mu M^{-1}s^{-1}$)	K_d(μM)	K_{pol}(s^{-1})	K_{pol}/K_d ($\mu M^{-1}s^{-1}$)	Selectivity[a]	K_d(μM)	K_{pol}(s^{-1})	K_{pol}/K_d ($\mu M^{-1}s^{-1}$)	Selectivity[a]
DNA/DNA	Wt RT	15.4±2.9	22.6±1.3	1.47	48.0±4.8	16.0±0.5	0.33	4.5	15.8±2.4	12.1±0.5	0.77	1.9
	M184V RT	73.2±8.0	22.4±0.9	0.31	605±285	29.8±10.4	0.05	6.2	168.1±25.6	18.9±1.1	0.11	2.8
DNA/RNA	Wt RT	67.1±10.2	65.0±3.9	0.97	40.8±9.2	18.4±1.4	0.45	2.2	11.4±2.7	11.7±0.8	1.0	0.97
	M184V RT	143.9±25.0	41.7±3.5	0.29	232.3±50.0	29.6±3.6	0.13	2.2	43.4±13.9	9.7±0.8	0.22	1.3

All values are mean ± SD.

[a] Selectivity is calculated by dividing the efficiency of dTTP (k_{pol}/K_d) by the efficiency of d4TTP or 4′-Ed4TTP.

the issue of whether the 4′-ethynyl d4TMP is one of the active metabolite instead of only 4′-ethynyl-d4TTP. Furthermore, 4′-ethynyl-stavudine is not a substrate for thymidylate phosphorlyase (TP) and may explain its pharmacokinetic advantages over stavudine [34].

In studies of intracellular metabolism of nucleoside analogs, the peak concentrations of the metabolites occurred at 2 h for zidovudine and at 12 h for both 4′-ethynylstavudine and stavudine. Interestingly, 4′-ethynylstavudine was phosphorylated to the triphosphate at a slower rate than that of stavudine, but faster than that of zidovudine. The amount of intracellular triphosphate metabolites of 4′-ethynylstavudine was higher than that of zudivudine at 24 h in culture [58]. The major metabolite of 4′-ethynylstavudine was the monophosphate, which contributed most to the linear increase in triphosphate over 12 hour. This was consistent with the behavior of 4′-ethynylstavudine toward TMP kinase, the rate limiting-step, observed previously [59]. Most importantly, 4′-Ed4TTP, the active metabolite, persisted significantly longer ($t_{1/2}$ 8.0 to 9.7 h) than diphosphate ($t_{1/2}$, 2.4 to 5.1 h) and monophosphate ($t_{1/2}$, 1.4 to 2.4 h) after removal of the drug from cell culture [57]. Further studies were done to find out whether the persistent intracellular 4′-Ed4TTP will translate to a more persistent anti-HIV-1 activity after removal of the drug from the culture medium. On the average, the ability of the inhibitors to protect cells from HIV infection after 48 h of removal of drug from cell culture was 4′-Ed4TTP > LFD4C > didanosine > stavudine > lamivudine > zidovudine > emtricitabine (FTC) > NVP [60]. That is, 4′-ethynylstavudine could protect uninfected cells against HIV replication longer than zidovudine, satavudine, and most of currently used HIV drugs. In a viral rebound studies, none of the inhibitors could completely prevent viral rebound after removal from culture. After 48 h of removal of inhibitor from cell culture, the fold-change in concentration of inhibitor required to keep viral rebound at 50% was in the order of didanosine < 4′-Ed4TTP < LFD4C < FTC < stavudine < lamivudine < NVP < zidovudine [61]. The persistence of antiviral activity of 4′-ethynylstavudine after removal of drug from culture may be due to; 1) the fact that the triphsphate once formed remains relatively stable and active in cells, and that the pool of the monophosphate (which is not effluxed out of the cells [60]) may continue to replenish the critical concentration of 4′-Ed4TTP, 2) less efficient removal of incorporated 4′-Ed4T by Exos from terminal viral DNA, and 3) inability of 4′-Ed4TTP metabolites to permeate the cell membrane [60] as compared to the metabolites of zidovudine [62].

In an initial selection for 4′-ethynylstavudine drug resistance study by Nitanda *et al.* [63] presented above, M184V mutation was observed on the 26th day and two additional mutations (P119S and T165A) of HIV RT were found on day 81. The M184V and triple (M184V/P119S/T165A) mutants were reported to confer 3-5-fold and 130-fold resistance to 4′-ethynylstavudine, respectively. This was puzzling as the P119S and/or T165A have not been observed previously in HIV-1-infected individuals. The clinical significance of these mutations was unknown. Several attempts at the Cheng lab to duplicate the initial selection for drug resistance failed (unpublished data). Therefore, the P119S, T165A, and M184V mutations were engineered into NL4-3 background to assess the contribution of each of these mutations to drug resistance, RT activity, and viral growth. Compared with wild type virus, variants with single RT mutations (P119S or T165A) did not show resistance to 4′- ethynylstavudine, however, the M184V and P119S/T165A/M184V strains conferred 3- and 5-fold resistance, respectively [56]. The P119S/M184V and T165A/M184V variants showed about 4-fold resistance to 4′-ethynylstavudine. The differences in the growth kinetics of the variants were less than 3-fold. The purified RT with P119S/M184V and T165A/M184V mutations were inhibited by 4′-Ed4TTP with 8 to13-fold less efficiency than wild type RT [55]. These findings led to reexamination of the viral strains from the original drug resistance selection. When the previous HIV resistant strain (P119S/T165A/M184V), with 130-fold resistance to 4′-ethynylstavudine, was recovered by Prof. Baba's lab from storage and cultured in the absence of 4′-ethynylstavudine for re-assessment of 4′-ethynylstavudine susceptibility, it was found to have only 3-5-fold resistance to 4′-Ed4T instead of the 130-fold resistance previously observed (Baba et. al., unpublished results). Could the previously observed 130-fold resistance of the P119S/T165A/M184V virus to 4′-ethynylstavudine be due to additional mutations in the RT and/or outside the RT sequence, or that this virus is either difficult to recover from storage due to a poor replication capacity? Based on recent studies and the structural modeling of interaction of HIV RT-primer complex and 4′-Ed4TTP, a virus with a high degree of resistance to 4′-ethynylstavudine (e.g., more that 50-fold resistance, highly resistant to 4′-ethynylstavudine) will be difficult to develop [57]. Mutations selected for during *in vitro* passage may not necessarily represent the mutation pathway that will evolve during clinical use, therefore, true resistance to 4′-ethynylstavudine is yet to be demonstrated in clinical studies. We surmise that clinical resistance to 4′-ethynylstavudine will be difficult to emerge in clinical studies with relevant dosage which will suppress M184V mutant virus, prerequisite for developing highly 4′-ethynylstavudine resistant virus if the initial resistance selection holds.

Interestingly, in pre-clinical studies by Oncolys BioPharma (Japan) 4′-ethynylstavudine was shown to be active against drug-resistant clinical isolates [35]. Moreover, the strains carrying the K65R or the Q151M complex were still susceptible to 4′-ethynylstavudine [34]. Furthermore, its efficacy against most isolates was at least equivalent to that of TDF. In a Phase Ia and Ib/IIa studies by Oncolys BioPharma (Japan), 4′-ethynylstavudine was well tolerated with no serious adverse events [63]. Early stage clinical studies suggest that 4′-ethynylstavudine is a promising candi-

date for HIV therapy. To date, the missing piece is whether resistance to 4′-ethynylstavudine will develop in the clinic. Ongoing and future clinical trials will inform on this.

CONFLICT OF INTEREST

The authors confirm that this article content has no conflicts of interest.

ACKNOWLEDGEMENTS

Financial supports from the Japan Society for the Promotion of Science (KAKENHI No. 21590123 and 24590144 to K. Haraguchi) are gratefully acknowledged. Also, this work was supported by Public Health Service grant AI-38204 from NIAID to Y.C.C. Y.C.C. is a fellow of the National Foundation for Cancer Research. E.P was supported by grant K08AI074404 from NIAID.

The authors are also grateful to Miss Y. Odanaka and Mrs. M. Matsubayashi (Center for Instrumental Analysis, Showa University) for technical assistance with NMR, MS, and elemental analyses.

REFERENCES

[1] Global report: UNAIDS report on the global AIDS endemic 2010. http://www.unaids.org/globalreport/global_report.htm. Accessed on 02/11/2012.

[2] Tan JJ, Chong XJ, Hu LM, Wang CX, Jia L, Liang XL. Therapeutic strategies underpinning the development of novel techniques for the treatment of HIV infection. Drug Discov. Today 2010; 15(5/6): 186-97.

[3] Matsuda A. Recent development of anti-HIV nucleosides. J Synth Org Chem Jpn 1990; 48(10): 907-20.

[4] Ichikawa E, Kato K. Sugar-modified nucleosides in past 10 years, a review. Current Medicinal Chemistry 2001; 8(4): 385-423.

[5] Huryn DM, Okabe M. AIDS-driven nucleoside chemistry. Chem Rev 1992; 92(8): 1745-68.

[6] De Clercq E. The design of drugs for HIV and HCV. Nature Review 2007; 6: 1001-18.

[7] McCarthy JR Jr, Robins RK, Robins MJ. Purine nucleosdes. XXII. synthesis of angustmycin A (decoynine) and related unsaturated nucleosides. J Am Chem Soc 1968; 90(17): 4993-9.

[8] Hattori H, Tanaka M, Fukushima M, Sasaki T, Matsuda A. Nucleosides and Nucleotides. 158. 1-(3-*C*-Ethynyl-β-D-ribo-pentofuranosyl)cytosine, 1-(3-*C*-ethynyl-β-D-ribo-pentofuranosyl)uracil and their nucleobase analogues as new potential multifunctional antitumor nucleosides with a broad spectrum of activity. J Med Chem 1996; 39(25): 5005-11.

[9] O-Yang C, Wu HY, Fraser-Smith EB, Walker KAM. Synthesis of 4′-cyanothymidine and analogs as potent inhibitors of HIV. Tetrahedron Lett 1992; 33(1): 37-40.

[10] Itoh Y, Haraguchi K, Tanaka H, Gen E, Miyasaka T. Divergent and stereocontrolled approach to the synthesis of uracil nucleosides branched at the anomeric position. J Org Chem 1995; 60(3): 656-62.

[11] Kodama T, Shuto S, Ichikawa S, Matsuda A. A highly stereoselective samarium diiodide-promoted aldol reaction with 1′-phenylseleno-2′-keto nucleosides. synthesis of 1′-α-branched uridine derivative. J Org Chem 2002; 67(22): 7706-15.

[12] Haraguchi K, Itoh Y, Matsumoto K, Nakamura KT, Tanaka H. Stereoselective synthesis of 1′-*C*-branched arabinofuranosyl nucleosides via anomeric radicals generated by 1,2-acyloxy migration. J Org Chem. 2003; 68(5): 2006-9.

[13] Kumamoto H, Murasaki M, Haraguchi K, Tanaka H. Nucleophilic addition of benzenethiol to 1′,2′-unsaturated nucleosides: 1′-*C*-phenylthio-2′-deoxynucleosides as anomeric radical precursors. J Org Chem. 2002; 67(17): 6124-30.

[14] Kodama T, Shuto S, Nomura M, Matsuda, A. An efficient method for the preparation of 1′ -branched-chain sugar pyrimidine ribonucleosides from uridine: the first conversion of a natural nucleoside into 1′-substituted ribonucleosides. Chem Eur J 2001; 7(12): 2332-40.

[15] Sugimoto I, Shuto S, Mori S, Shigeta S, Matsuda A. Nucleosides and nucleotides. 183. synthesis of 4′α-branched thymidines as a new type of antiviral agent. Bioorg Med Chem Lett.1999; 9(3): 385-8.

[16] For a review, see: Smith JG. Synthetically useful reactions of epoxides. Synthesis 1984; 629-56.

[17] Ashwell M, Jones AS, Walker RT. The synthesis of some branched-chain-sugar nucleoside analogues. Nucleic Acids Res 1987; 15(5): 2157-66.

[18] Adam W, Balas J, Hadjarapoglou L. A convenient preparation of acetone solution of dimethyldioxirane., Chem Ber 1991; 124(10): 2377.

[19] Curci R, Fiorentiono M, Troisi L, Edwards JO, Pater RH. Epoxidation of alkenes by dioxirane intermediates generated in the reaction of potassium caroate with ketones. J Org Chem 1980; 45(23): 4758-60.

[20] Murray RW, Jeyaman R. Dioxiranes: synthesis and reaction of methyldioxiranes. J Org Chem 1985; 50(16): 2847-53.

[21] Haraguchi K, Kubota Y, Tanaka H. Ring opening of nucleoside 1′,2′-epoxides with organoaluminum reagents: stereoselective entry to ribonucleosides branched at the anomeric position. J Org Chem 2004; 69(6): 1831-6.

[22] Haraguchi K, Konno K, Yamada K, Kitagawa Y, Nakamura KT, Tanaka H. Electrophilic glycosidation employing 3,5-*O*-(di-*tert*-butylsilylene)-*erythro*-furanoid glycal leads to exclusive formation of the β-anomer: synthesis of 2′-deoxynucleosides and its 1′-branched analogues. Tetrahedron 2010; 66(25): 4587-600.

[23] Kubota Y, Haraguchi K, Kunikata M, Hayashi M, Ohkawa M, Tanaka H. Anti versus syn opening of epoxides derived from 9-(3-deoxy-β-D-*glycero*-pento-3-enofuranosyl)adenine with Me_3Al : factors controlling the stereoselectivity. J Org Chem 2006; 71(3): 1099-103.

[24] Maag H, Rydzewski RM, McRoberts MJ, Crawford-Ruth D, Verheyden JPH, Prisbe EJ. Synthesis and anti-HIV activity of 4′-azido- and 4′-methoxynucleosides. J Med Chem 1992; 35(8): 1440-51.

[25] O-Yang C, Wu HY, Fraser-Smith EB, Walker KAM. Synthesis of 4′-cyanothymidine and analogs as potent inhibitors of HIV. Tetrahedron Lett 1992; 33(1): 37-40.

[26] Sugimoto I, Shuto S, Mori S, Shigeta S, Matsuda A. Synthesis of 4′-α-branched thymidines as a new type of antiviral agent. Bioorg Med Chem Lett 1999; 9(3): 385-8.

[27] Nomura M, Shuto S, Tanaka M, *et al.* Synthesis and biological activities of 4′-α-branched-chain sugar pyrimidine nucleosides J Med Chem 1999; 42(15): 2901-8.

[28] Ohrui H, Kohgo S, Kitano K, *et al.* Synthesis of 4′-*C*-ethynyl -D-arabino- and 4′-*C*-ethynyl-2′-deoxy-β-D-ribo-pentofuranosyl-pyrimidines and –purines and evaluation of their anti-HIV activity. J Med Chem 2000; 43(23); 4516-25.

[29] Kodama E, Kohgo S, Kitano K, *et al.* 4′-Ethynyl nucleoside analogs: potent inhibitors of multidrug-resistant human immunodeficiency virus varinats *in vitro*. Antimicrob Agents Chemother 2001; 45(5): 1539-46.

[30] Nomura S, Shuto S, Tanaka M, *et al.* Synthesis and biological activity of 4′-alpha-*C*-branched-chain-sugar pyrimidine nucleosides J Med Chem 1999; 42(15); 2901-8.

[31] Ohrui H, Kohgo S, Kitano K, *et al.* Synthesis of 4′-*C*-ethynyl beta-D-arabino and 4′-*C*-ethynyl-beta-D-ribo-pentofuranosylpyrimidine and -purines and evaluation of their anti-HIV activity. J Med Chem 2000; 43(23): 4516-25.

[32] Haraguchi K, Takeda S, Tanaka H. Ring opening of 4′,5′-epoxynucleosides: a novel stereoselective entry to 4′-*C*-branched nucleosides. Org Lett 2003; 5(9): 1399-402.

[33] Haraguchi K, Takeda S, Tanaka H, *et al.* Synthesis of a highly active new anti-HIV agent 2′,3′-didehydro-3′-deoxy-4′-ethynylthymidine. Bioorg Med Chem Lett 2003; 13(19): 3775-7.

[34] Dutschman GE, Grill SP, Gullen EA, *et al.* Novel 4′-substituted stavudine analog with improved anti-human immunodeficiency virus activity and decreased cytotoxicity. Antimicrob Agents Chemother 2004; 48(5): 1640-6.

[35] Nitanda T, Wang X, Kumamoto H, *et al.* Anti-human immunodeficiency virus type 1 activity and resistance profile of 2′,3′-didehydro-3′-deoxy-4′-ethynylthymidine *in vitro*. Antimicrob Agents Chemother 2005; 49(8): 3355-60.

[36] Haraguchi K, Itoh Y, Takeda S, *et al.* Synthesis and anti-HIV activity of 4′-cyano-2′,3′-didehydro-3′-deoxythymidine. Nucleosdes Nucletides Nucleic Acids 2004; 23(4): 647-4.

[37] Tanaka H, Haraguchi K, Kumamoto H, Baba M, Cheng YC. 4′-ethynylstavudine (4′-Ed4T) has potent anti-HIV activity with reduced toxicity and shows a unique activity profile against drug-

resistant mutants. Antiviral Chemistry & Chemotherapy 2005; 16(4): 217-21.

[38] Kumamoto H, Haraguchi K, Tanaka H, *et al.* Synthesis of (±)-4′-ehtynyl- and 4′-cyano carbocyclic analogues of stavudine (d4T). Nucleosides Nucleotides Nucleic Acids 2005; 24(2): 73-83.

[39] Kumamoto H, Haraguchi K, Ida M, *et al.* Synthesis of (±)-4′-ehtynyl-5′,5′-difluoro-2′,3′-dehydro-3′-deoxy-carbocyclic thymidine: a difluoromethylidene analogue of promising anti-HIV agent Ed4T. Tetrahedron 2009; 65(36): 7630-6.

[40] Kumamoto H, Nakai T, Haraguchi K, *et al.* Synthesis and anti-HIV-1 activity of 4′-branched (±)-4′-thiostavudines. J Med Chem. 2006; 49(26): 7861-67.

[41] Larder BA, Kemp SD, Multiple mutations in HIV-1 reverse transcriptase confer high-level resistance to zidovudine (AZT). Science, 1989; 246(4934): 1155-8.

[42] Schinazi RF, Lloyd RM Jr, Nguyen MH, *et al.* Characterization of human immunodeficiency viruses resistant to oxathiolane-cytosine nucleosides. Antimicrob Agents Chemother 1993; 37(4): 875-81.

[43] Margot NA, Isaacson E, McGowan I, Cheng A, Miller MD. Extended treatment with tenofovir disoproxil fumarate in treatment-experienced HIV-1-infected patients: genotypic, phenotypic, and rebound analyses. J Acquir Immune Defic Syndr. 2003; 33(1): 15-21.

[44] Miller MD. K65R, TAMs and tenofovir. AIDS Rev. 2004; 6(1): 22-33.

[45] White KL, Margot NA, Wrin T, Petropoulos CJ, Miller MD, Naeger LK. RT processivities *in vitro*, consistent with a potential fitness defect *in vivo* and the low prevalence of the K65R mutation among isolates from antiretroviral agent-experienced patients. Antimicrob Agents Chemother. 2002; 46(10): 3437-46.

[46] Shirasaka T, Kavlick MF, Ueno T, *et al.* Emergence of human immunodeficiency virus type 1 variants with resistance to multiple dideoxynucleosides in patients receiving therapy with dideoxynucleosides. Proc Natl Acad Sci U S A 1995; 92(6): 2398-402.

[47] Delviks-Frankenberry, KA, Nikolenko GN, Barr R, Pathak VK. Mutations in human immunodeficiency virus type 1 RNase H primer grip enhance 3′-azido-3′-deoxythymidine resistance. J Virol. 2007; 81(13): 6837-45.

[48] Nikolenko GN, Delviks-Frankenberry KA, Palmer S, *et al.* Mutations in the connection domain of HIV-1 reverse transcriptase increase 3′-azido-3′-deoxythymidine resistance. Proc Natl Acad Sci U S A. 2007; 104(1): 317-22.

[49] Hachiya A, Kodama EN, Sarafianos SG, *et al.* Amino acid mutation N348I in the connection subdomain of human immunodeficiency virus type 1 reverse transcriptase confers multiclass resistance to nucleoside and nonnucleoside reverse transcriptase inhibitors. J Virol. 2008; 82(7); 3261-70.

[50] Yap SH, Sheen, CW, *et al.* N348I in the Connection Domain of HIV-1 Reverse Transcriptase Confers Zidovudine and Nevirapine Resistance. PLoS Med 2007; 4: e335.

[51] Ehteshami M, Beilhartz GL, Scarth BJ, *et al.* Connection domain mutations N348I and A360V in HIV-1 reverse transcriptase enhance resistance to 3'-azido-3'-deoxythymidine through both RNase H-dependent and -independent mechanisms J Biol Chem 2008; 283(32): 22222-32.

[52] Longley MJ, Ropp PA, Lim SE, Copeland WC. Characterization of the native and recombinant catalytic subunit of human DNA polymerase gamma: identification of residues critical for exonuclease activity and dideoxynucleotide sensitivity. Biochemistry 1998; 37(29): 10529-39.

[53] Chen CH, Cheng YC. Delayed cytotoxicity and selective loss of mitochondrial DNA in cells treated with the anti-human immunodeficiency virus compound 2′,3′-dideoxycytidine. J Biol Chem 1989; 264(20): 11934-7.

[54] Chen CH, Vazquez-Padua M, Cheng YC. Effect of anti-human immunodeficiency virus nucleoside analogs on mitochondrial DNA and its implication for delayed toxicity. Mol Pharmacol. 1991; 39(5): 625-8.

[55] Yang G, Dutschman GE, Wang CJ, *et al.* Highly selective action of triphosphate metabolite of 4′-ethynyl D4T: a novel anti-HIV compound against HIV-1 RT. Antiviral Res 2007; 73(3): 185-91.

[56] Yang G, Wang J, Cheng Y, *et al.* Mechanism of inhibition of human immunodeficiency virus type 1 reverse transcriptase by a stavudine analogue, 4′-ethynyl stavudine triphosphate. Antimicrob Agents Chemother 2008; 52(6): 2035-42.

[57] Yang G, Paintsil E, Dutschman GE, *et al.* Impact of Novel HIV-1 Reverse Transcriptase Mutations, P119S and T165A on 4′-ethynyl-thymidine Analog Resistance Profile. Antimicrob Agents and Chemother 2009; 53(11); 4640-6.

[58] Paintsil E, Dutschman GE, Hu R, *et al.* Intracellular metabolism and persistence of the anti-human immunodeficiency virus activity of 2′,3′-didehydro-3′-deoxy-4′-ethynylthymidine, a novel thymidine analog. Antimicrob Agents Chemother 2007; 51(11): 3870-9.

[59] Hsu CH, Hu R, Dutschman GE, *et al.* Comparison of the phosphorylation of 4′-ethynyl 2′,3′-dihydro-3′-deoxythymidine with that of other anti-human immunodeficiency virus thymidine analogs. Antimicrob Agents Chemother 2007; 51(5): 1687-93.

[60] Wang X, Tanaka H, Baba M, Cheng YC. Study of the retention of metabolites of 4′-Ed4T, a novel anti-HIV-1 thymidine analog, in cells. Antimicrob Agents Chemother 2009; 53(8): 3317-24.

[61] Paintsil E, Grill SP, Dutschman GE, Cheng YC. Comparative study of the persistence of anti-HIV activity of deoxynucleoside HIV reverse transcriptase inhibitors after removal from culture. AIDS Res Ther 2009; 6: 5.

[62] Zimmerman TP, Mahony WB, Prus KL. 3′-azido-3′-deoxythymidine. An unusual nucleoside analogue that permeates the membrane of human erythrocytes and lymphocytes by nonfacilitated diffusion. J Biol Chem 1987; 262(12): 5748-54.

[63] Takuma Mastuda, Elijah Paintsil, Joel S. Ross, Jessica Schofield, Yung-Chi Cheng, Yasuo Urata. A Single Dose Escalation Study to Evaluate the Safety, Tolerability, and Pharmacokinetics of OBP-601 (4′-Ed4T a Novel NRTI) in Healthy Subjects. 16th Conference on Retroviruses and Opportunistic Infections. Montreal, Canada; 2009.

Received: September 6, 2012 **Accepted: October 10, 2012**

Published online 8 September 2011

Nucleic Acids Research, 2012, Vol. 40, No. 1 ***345–359***
doi:10.1093/nar/gkr694

Biochemical, inhibition and inhibitor resistance studies of xenotropic murine leukemia virus-related virus reverse transcriptase

Tanyaradzwa P. Ndongwe[1], Adeyemi O. Adedeji[1], Eleftherios Michailidis[1], Yee Tsuey Ong[1], Atsuko Hachiya[1], Bruno Marchand[1], Emily M. Ryan[1], Devendra K. Rai[1], Karen A. Kirby[1], Angela S. Whatley[1], Donald H. Burke[1,2], Marc Johnson[1], Shilei Ding[3], Yi-Min Zheng[1], Shan-Lu Liu[1,3], Ei-Ichi Kodama[4], Krista A. Delviks-Frankenberry[5], Vinay K. Pathak[5], Hiroaki Mitsuya[6], Michael A. Parniak[7], Kamalendra Singh[1] and Stefan G. Sarafianos[1,2,*]

[1]Christopher Bond Life Sciences Center, Department of Molecular Microbiology & Immunology, University of Missouri, School of Medicine, Columbia, [2]Department of Biochemistry, University of Missouri, Columbia, MO 65211, USA, [3]Department of Microbiology and Immunology, McGill University, Montreal, QC, Canada, [4]Department of Internal Medicine, Division of Emerging Infectious Diseases, Tohoku University School of Medicine, Sendai, Japan, [5]HIV Drug Resistance Program, National Cancer Institute-Frederick, Frederick MD, [6]Department of Internal Medicine, Kumamoto University School of Medicine, Kumamoto Japan & Experimental Retrovirology Section, HIV/AIDS Malignancy Branch, NIH, Bethesda MD and [7]Department of Molecular Genetics & Biochemistry, University of Pittsburgh School of Medicine, Pittsburgh, PA, USA

Received June 3, 2011; Revised August 5, 2011; Accepted August 8, 2011

ABSTRACT

We report key mechanistic differences between the reverse transcriptases (RT) of human immunodeficiency virus type-1 (HIV-1) and of xenotropic murine leukemia virus-related virus (XMRV), a gammaretrovirus that can infect human cells. Steady and pre-steady state kinetics demonstrated that XMRV RT is significantly less efficient in DNA synthesis and in unblocking chain-terminated primers. Surface plasmon resonance experiments showed that the gammaretroviral enzyme has a remarkably higher dissociation rate (k_{off}) from DNA, which also results in lower processivity than HIV-1 RT. Transient kinetics of mismatch incorporation revealed that XMRV RT has higher fidelity than HIV-1 RT. We identified RNA aptamers that potently inhibit XMRV, but not HIV-1 RT. XMRV RT is highly susceptible to some nucleoside RT inhibitors, including Translocation Deficient RT inhibitors, but not to non-nucleoside RT inhibitors. We demonstrated that XMRV RT mutants K103R and Q190M, which are equivalent to HIV-1 mutants that are resistant to tenofovir (K65R) and AZT (Q151M), are also resistant to the respective drugs, suggesting that XMRV can acquire resistance to these compounds through the decreased incorporation mechanism reported in HIV-1.

INTRODUCTION

Xenotropic murine leukemia virus-related virus (XMRV) is a gammaretrovirus that was first identified in some prostate cancer tissues (1,2) While some subsequent reports confirmed the presence of XMRV in prostate cancer samples (3–6), several others found little or no evidence of the virus in patient samples (7–9). XMRV DNA was also reported in 67% of patients with chronic fatigue syndrome (CFS) (10), but several subsequent studies in Europe and the USA failed to identify XMRV DNA in CFS patients or healthy controls (11–15). Hence, the relevance of XMRV to human disease remains unclear (16) and have been challenged (17). Most recently, it has been reported that XMRV has been generated through recombination of two separate proviruses suggesting that the association of XMRV with human disease is due to contamination of human samples with virus originating from this recombination event (18). Nonetheless, as a retrovirus that can infect human cells, XMRV can be very helpful in advancing our understanding of the mechanisms of retroviral reverse transcription, inhibition and drug resistance.

*To whom correspondence should be addressed. Tel: +1 573 882 4338; Fax: +1 573 884 9676; Email: sarafianoss@missouri.edu

XMRV RT is similar to the Moloney murine leukemia virus (MoMLV) RT, which has been the subject of structural and biochemical studies (19–24). Most of the differences between these gammaretroviral enzymes are at the RNase H domain (Supplementary Figure S1). Comparisons of human immunodeficiency virus type-1 (HIV) RT with MoMLV RT have revealed structural and sequence differences (21). For example, HIV-1 RT is a heterodimer composed of two related subunits (25,26) [reviewed in (27,28)]. Its larger p66 subunit (~66 kDa) contains both the polymerase and RNase H domains; the smaller p51 subunit, (~51 kDa), is derived from the p66 subunit by proteolytic cleavage and its role is to provide structural support and optimize RT's biochemical functions (29). In contrast, structural studies have demonstrated that MoMLV RT is a monomer of about 74 kDa, although one study reported that it may form a homodimer during DNA synthesis (30). So far, there are no published biochemical or structural studies on XMRV RT. Hence, the present study on this enzyme and its comparison to related enzymes provides an excellent opportunity to advance our biochemical understanding of the mechanism of reverse transcription, its inhibition and drug resistance.

MATERIALS AND METHODS

Expression and purification of XMRV, HIV-1 and MoMLV RTs

The plasmid pBSK-XMRV containing the coding sequence of XMRV RT from the VP62 clone (GenBank: DQ399707.1) was chemically synthesized and optimized for bacterial expression by Epoch Biolabs Inc (Missouri City, Texas, USA). The 2013 bp XMRV RT sequence was amplified from pBSK-XMRVRT by PCR, using the forward and reverse primers 1 (all primer sequences are shown in Supplementary Table S1), resulting in NdeI and HindIII restriction sites. Drug resistant XMRV RT mutants Q190M and K103R (equivalent to HIV-1 Q151M RT and K65R) were generated by site-directed mutagenesis using forward and reverse primers 2 and 3. The digested amplicons were ligated into pET-28a (Novagen), resulting into a construct that expresses an N-terminal hexahistidine tag. pET-28a-MRT encoding full-length wild-type MoMLV RT was provided by Dr M. Modak (New Jersey Medical School, Newark NJ, USA).

Expression and purification of MoMLV and XMRV RTs were carried out similarly to our previously published protocols (23,24). Briefly, RTs were expressed in BL21-pLysS *Escherichia coli* (Invitrogen) grown at 37°C and induced with 150 μM IPTG at OD_{600} 0.8, followed by 16 h growth at 17°C. A cell pellet from a 3 l culture was incubated with 40 ml lysis buffer (50 mM Tris–HCl, pH 7.8, 500 mM NaCl, 1 mM PMSF, 0.1% NP-40, 1% sucrose and 2 mg/ml lysozyme), then sonicated and centrifuged at 15,000 *g* for 30 min. The supernatant was diluted 2-fold in Buffer A (50 mM Tri–HCl pH 7.8, 1 mM PMSF, 4% streptomycin sulfate and 10% sucrose), stirred on ice for 30 min and centrifuged. The supernatant was loaded on a Ni-NTA column and bound proteins were washed with 20 ml Buffer B (20 mM Tris–HCl pH 7.5, 500 mM NaCl) and 5 mM imidazole, followed by 20 ml Buffer B with 75 mM imidazole. RT was eluted in 2 ml fractions with 20 ml buffer B containing 300 mM imidazole. Fractions with RT were pooled and further purified by size exclusion chromatography (Superdex 75; GE Healthcare). RTs (>95% pure) were stored in 50 mM Tris–HCl pH 7.0, 100 mM NaCl, 1 mM DTT, 0.1% NP-40 and 30% glycerol in 10 μl aliquots at −20°C. Protein concentrations were determined by measuring UV_{280} (molar extinction coefficients of 106 and 103 $M^{-1}cm^{-1}$ for XMRV and MoMLV RT).

HIV-1 RT was cloned in a pETduo vector and purified as described previously (29,31,32). Oligonucleotide sequences (IDT-Coralville, IA, USA) of DNA/RNA substrates are shown in Supplementary Table S1. Nucleotides were purchased from Fermentas (Glen Burnie, MD, USA). They were treated with inorganic pyrophosphatase (Roche Diagnostics, Mannheim, Germany) as described previously (33) to remove PPi that might interfere with excision assays.

Steady state kinetics

Steady state parameters K_m and k_{cat} for dATP incorporation were determined using single nucleotide incorporation gel-based assays. XMRV RT and MoMLV RT reactions were carried out in 50 mM Tris–HCl pH 7.8, 60 mM KCl, 0.1 mM DTT, 0.01% NP-40 and 0.01% bovine serum albumin (BSA) (Reaction Buffer) with 6 mM $MgCl_2$ or 1.5 mM $MnCl_2$, 0.5 mM EDTA, 200 nM or 100 nM T_{d26}/5′-Cy3-P_{d18b}, 20 nM or 5 nM RT for XMRV and MoMLV RTs, respectively and varying concentrations of dNTP in a final volume of 10 μl. The reactions for HIV-1 RT were carried out in Reaction Buffer with 100 nM T_{d26}/5′-Cy3-P_{d18b}, 10 nM HIV-1 RT and 6 mM $MgCl_2$ in a 20 μl reaction. All the concentrations mentioned here and in subsequent assays reflect final concentration of reactants otherwise mentioned reactions were stopped after 15 min for XMRV, 4 min for MoMLV RT, and 2.5 min for HIV-1. The products were resolved on 15% polyacrylamide–7M urea gels. The gels were scanned with a Fuji Fla-5000 PhosphorImager (Stamford, CT, USA) and the bands were quantified using MultiGauge. Results were plotted using GraphPad Prism 4. K_m and k_{cat} were determined graphically using Michaelis–Menten equation.

Gel mobility shift assays

Formation of RT-DNA binary complex: 20 nM T_{d31}/5′-Cy3-P_{d18a} (Supplementary Table S1) was incubated for 10 minutes with increasing amounts of MoMLV or XMRV RT in 50 mM Tris–HCl pH 7.8, 0.01% BSA, 5 mM $MgCl_2$ and 10% (v/v) sucrose. The complexes were resolved on native 6% polyacrylamide 50 mM Tris–borate gel and visualized as described above.

Active site titration and determination of $K_{D.DNA}$

Active site concentrations and kinetic constants of DNA binding for XMRV, HIV-1 and MoMLV RTs were determined using pre-steady state experiments. Reactions

with XMRV and MoMLV RTs were carried out in the reaction buffers listed above. For XMRV RT 100 nM protein was pre-incubated with increasing concentrations of T_{d31}/5′-Cy3-P_{d18a}, followed by rapid mixing with a reaction mixture containing 5 mM $MgCl_2$ and 100 μM next incoming nucleotide (dATP). The reactions were quenched at various times (5 ms to 4 s) by adding EDTA to a final concentration of 50 mM. The amounts of 19-mer product were quantified and plotted against time. The data were fit to the following burst equation:

$$P = A(1 - e^{-k_{obs}t}) + k_{ss}t \quad (1)$$

where A is the amplitude of the burst phase that represents the RT–DNA complex at the start of the reaction, k_{obs} is the observed burst rate constant for dNTP incorporation, k_{ss} is the steady state rate constant and t is the reaction time. The rate constant of the linear phase (k_{cat}) was estimated by dividing the slope of the linear phase by the enzyme concentration. The active site concentration and T/P binding affinity ($K_{D.DNA}$) were determined by plotting the amplitude (A) against the concentration of T/P. Data were fit to the quadratic equation (Equation 2) using non-linear regression:

$$A = 0.5(K_D + [RT] + [DNA] - \sqrt{0.25(K_D + [RT] + [DNA])^2} - ([RT] + [DNA]) \quad (2)$$

where K_D is the dissociation constant for the RT–DNA complex, and [RT] is the concentration of active polymerase. HIV-1 RT's DNA binding affinity was determined as previously described (29).

Surface plasmon resonance assay

We used surface plasmon resonance (SPR) to measure the binding constants of XMRV and HIV-1 RTs to double-stranded DNA. Experiments were carried out using a Biacore T100 (GE Healthcare). To prepare the sensor chip surface we used the 5′-biotin-T_{d37}/P_{d25} oligonucleotide (Supplementary Table S1). One hundred and twenty RUs of this DNA duplex were bound in channel 2 of a streptavidin-coated sensor chip [Series S Sensor Chip SA (certified)] by flowing a solution of 0.1 μM DNA at a flow rate of 10 μl/min in a buffer containing 50 mM Tris pH 7.8, 50 mM NaCl. The binding constants were determined as follows: RT binding was observed by flowing solutions containing increasing concentrations of the enzyme (0.2, 0.5, 1, 2, 5, 10, 20, 50, 100 and 200 nM) in 50 mM Tris pH 7.8, 60 mM KCl, 1 mM DTT, 0.01% NP40 and 10 mM $MgCl_2$ in channels 1 (background) and 2 (test sample) at 30 μl/min. The trace obtained in channel 1 was subtracted from the trace in channel 2 to obtain the binding signal of RT. This signal was analyzed using the Biacore T100 Evaluation software to determine $K_{D.DNA}$, k_{on} and k_{off}.

Pre-steady state kinetics of dNTP incorporation

The optimal nucleotide incorporation rates (k_{pol}) were obtained by pre-steady state kinetics analysis using single nucleotide incorporation assays. A solution containing XMRV RT (150 nM final concentration) and T_{d31}/5′-Cy3-P_{d18a} (40 nM) was rapidly mixed with a solution of $MgCl_2$ (5 mM) and varying dATP (5–200 μM) for 0.1 to 6 s before quenching with EDTA (50 mM) (all concentrations in parentheses are final, unless otherwise stated). Products were resolved and quantified as described above. Burst phase incorporation rates and substrate affinities were obtained from fitting the data to Equation 1. Turnover rates (k_{pol}), dNTP binding to the RT-DNA complex ($K_{d.dATP}$), and observed burst rates (k_{obs}) were fit to the hyperbolic equation:

$$k_{obs} = (k_{pol}[dNTP])/(K_{d.dNTP} + [dNTP]) \quad (3)$$

HIV-1 RT's DNA binding affinity was determined as previously described (29).

Fidelity of DNA synthesis

The fidelity (error-proneness) of XMRV RT was determined and compared with that of MoMLV RT and HIV-1 RT by primer extension assays using 10 nM heteropolymeric T_{d100}/5′-Cy3-P_{d18a}. Reactions (10 μl) were carried out in Reaction Buffer containing all four dNTPs (100 μM each) or only three dNTPs (missing either dATP, dGTP or dTTP) at 100 μM each. Incubations of the XMRV and MoMLV (50 nM) reactions were at 37°C for 45 min and 30 min for HIV-1 RT (20 nM). Reactions were initiated by adding dNTPs, stopped with equal volume of formamide-bromophenol blue, and an aliquot was run on a 16% polyacrylamide–7M urea gel.

Kinetics of mismatch incorporation

For these experiments, instead of including the next correct nucleotide (dATP) in the polymerase reactions, we used dTTP as the mismatched incoming nucleotide. Hence, 50 nM XMRV RT was pre-incubated with 35 nM T_{d31}/5′-Cy3-P_{d18a} in reaction mixture. Reactions were initiated by adding dTTP (5–750 μM) and 5 mM $MgCl_2$, followed by incubation (37°C) for 5 min, due to the decreased mismatch incorporation rate of XMRV. For MoMLV RT, 30 nM RT and 20 nM DNA used and the reactions were carried out for 2.5 minutes. For HIV-1, 30 nM RT, 20 nM DNA and 0–200 μM nucleotide were used and the reactions were carried out for 2.5 min. The amount of extended primer was quantified and plotted against the concentration of dTTP. The data were used to derive the $K_{d.dNTP}$ of incorrect nucleotide binding, the rate k_{pol} (using Equations 1 and 3) and the efficiency of the misincorporation reaction ($k_{pol}/K_{d.dTTP}$).

Determination of *in vivo* fidelity

ANGIE P cells, which contain a retroviral vector (GA-1) that encodes a bacterial β-galactosidase gene (*lacZ*) and a neomycin phosphotransferase gene, were plated (5×10^6 cells/100 mm dish) and after 24 h were transfected using the calcium phosphate precipitation method with a plasmid expressing either XMRV or amphotropic MLV (AM-MLV) (three independent transfections per vector). After 48 h, the culture medium with XMRV or (AM-MLV) was harvested, serially diluted and used to infect

D17 target cells (2×10^5 cells/60 mm dish) in the presence of polybrene. The infected D17 cells were selected for resistance to G418 (400 μg/ml) in the presence of 1 μM AZT to suppress reinfection, and characterized by staining with 5-bromo-4-chloro-3-indoyl-β-D-galacto-pyranoside (X-Gal) ~2 weeks after G418 selection. The frequencies of inactivating mutations in *lacZ* quantified as described before (blue versus white colonies) (34).

Processivity of DNA synthesis—trap assay

Processivity reactions were carried out in Reaction Buffer containing 20 nM T_{d100}/P_{d18}, 100 μM of each dNTP, 30 nM HIV-1 RT, 50 nM MoMLV RT or 100 nM XMRV RT and 1μg/μl unlabeled calf thymus DNA trap in 50 μL. Enzymes were pre-incubated with T_{d100}/P_{d18} for 1 min before adding dNTPs (100 μM each) together with the calf thymus DNA trap. Reactions were incubated at 37°C, and 10 μl aliquots were taken out at 3, 7.5 and 15 min for HIV-1 RT or at 7.5, 15 and 30 min for XMRV RT and MoMLV RT, and mixed with equal volume of loading dye. The effectiveness of the trap was determined by pre-incubating the enzyme with the trap before adding T_{d100}/P_{d18}. Control DNA synthesis was measured in absence of trap under the same conditions. Reaction products were resolved as above.

Single turnover processivity assays

Thirty nanomolar $T_{d31}/5'$-Cy3-P_{d18a} was pre-incubated for 10 min with 100 nM XMRV or 50 nM MoMLV RT in Reaction Buffer, then rapidly mixed with 100 μM dNTPs, 5 mM $MgCl_2$ for varying times (0.1–45 s) before quenching with EDTA (50 mM final). Single turnover processivity of HIV-1 RT was assayed with 40 nM enzyme, 20 nM DNA and 50 μM of each nucleotide were used. The reaction products were resolved and quantified as described above. The data were fit to a one-phase exponential decay equation for the elongation of the 18-mer primer. The rates of appearance and extension of products from subsequent nucleotide incorporations (19- and 27-mer) were obtained by fitting the intensities of corresponding bands to double exponential (Equation 4):

$$P = A(1 - e^{-k_1 t}) + (e^{-k_2 t}) + C \quad (4)$$

where A is the amplitude, P is the amount of 19-mer, 20-mer or higher length products, k_1 is the rate of product generation, k_2 the rate of subsequent elongation and C a constant (29,35).

Assays for reverse transcriptase inhibition

DNA synthesis by 50 nM XMRV RT or MoMLV RT was carried out in Reaction Buffer using 20 nM $T_{d100}/5'$-Cy3-P_{d18a}, 2.5 μM dNTP, 5 mM $MgCl_2$ and varying amounts of NRTI (0–100 μM). Reactions were quenched with 95% formamide after 1 h incubation at 37°C (38). In experiments with aptamers 10 nM XMRV RT, 20 nM $T_{d31}/5'$-Cy3-P_{d18a} and 50 μM dNTPs were used in the presence of varying amounts of aptamer for 30 min (0–500 nM for m.1.3; 0–25 nM for m.1.4 and m.1.1FL). The inhibition of DNA polymerization was monitored by resolving the products on 15% polyacrylamide–7 M urea gels and visualized as described above. Bands corresponding to full extension products were quantified using MultiGauge Software and IC_{50}s were obtained from dose–response curves using GraphPad Prism.

PPi- and ATP-dependent excision and rescue of $T/P_{AZT\text{-}MP}$ or $T/P_{EFdA\text{-}MP}$

The ability of enzymes to use PPi or ATP to unblock template-primers that had AZT-MP ($T/P_{AZT\text{-}MP}$) or EFdA-MP ($T/P_{EFdA\text{-}MP}$) at their 3′ primer ends was measured as follows: 20 nM of $T/P_{AZT\text{-}MP}$ or $T/P_{EFdA\text{-}MP}$ were prepared as described before (32). They were incubated at 37°C with either 60 nM HIV-1 RT or 200 nM XMRV RT in the presence of 0.15 mM PPi or 3.5 mM ATP for PPi- or ATP-dependent rescue reactions, respectively. Reactions were initiated by the addition of $MgCl_2$ (6 mM). Aliquots were removed at different times (0–90 min) and analyzed as above. Rescue assays were performed in the presence of 100 μM dATP to prevent EFdA-MP reincorporation, 0.5 μM dTTP, 10 μM ddGTP and 10 mM $MgCl_2$.

Molecular modeling

The sequence of XMRV RT from the VP62 clone was aligned with that of MoMLV RT (PDB: 1RW3) (21,22) using ClustalW. To generate the homology model of XMRV RT, we used the Prime protocol of the Schrödinger software suite (Schrödinger Inc. NY). The resulting molecular model was further energy minimized by OPLS2005 force field using the Impact option of Schrödinger. The final model was validated with PROCHECK v.3.5.4.

RESULTS

Comparison of RT sequences

The XMRV and MoMLV enzymes are closely related (~95% sequence identity) with most of the differences between them being in the RNase H domain (Supplementary Figure S1). While XMRV and MoMLV differ significantly from HIV-1 RT, the known polymerase motifs (A–F) are well conserved in all three enzymes (Supplementary Figure S1). Specifically, the active site aspartates in Motifs A and C (Figure 9) (D150, D224, D225 in XMRV RT; D150, D224, D225 in MoMLV RT; D110, D185, D186 in HIV-1 RT) are conserved in all three RTs. Also, the three enzymes are similar in Motif B, which is involved in dNTP binding and multidrug resistance (AZT and dideoxy-nucleoside drugs) through the decreased incorporation mechanism (27,39–41). Specifically, all three enzymes have a glutamine at the start of this motif (Q151 in HIV-1 RT, Q190 in XMRV RT and Q190 in MoMLV RT). Motif D includes HIV-1 RT residues L210 and T215, which when mutated they enhance excision of AZT from the AZT-terminated primer terminus. This motif is mostly different in XMRV and MoMLV RTs, where the corresponding residues are N226 and A231 (Supplementary Figure S1). K219 of HIV-1 RT Motif D is proximal to

the dNTP-binding pocket and is also conserved in the other enzymes (K235). The DNA primer grip (Motif E) (36,42) in HIV-1 RT ($M_{230}G_{231}Y_{232}$) is slightly different in the gammaretroviral enzymes ($L_{245}G_{246}Y_{247}$). Motif F at the fingers subdomain of all enzymes has two conserved lysines that bind the triphosphate of the dNTP (K65 and K72 in HIV-1 RT; K103 and K110 in XMRV and MoMLV RTs).

Several HIV-1 residues involved in NRTI resistance have the resistance mutations in XMRV and MoMLV RTs (Table 1). Hence, XMRV and MoMLV RTs have a Val as the X residue (codon 223) of the conserved YXDD sequence of Motif C. An M184V mutation at this position in HIV-1 RT causes strong, steric hindrance-based, resistance to 3TC and FTC (43–45), and to a lesser extent to ddI, ABC [reviewed in (46)], and translocation defective RT inhibitors (TDRTIs) (43) (Table 1). Similarly, the M41L mutation, which causes excision-based AZT resistance in HIV is already present in XMRV and MoMLV RT (L81, Table 1). The gammaretroviral enzymes differ from HIV-1 RT in several other HIV drug resistance sites (HIV residues 62, 67, 69, 70, 75, 77, 115, 210, 215) (Table 1). Finally, there are also differences in residues that are essential for NNRTI binding in HIV-1 RT: W229 changes to Y268 in XMRV RT, Y181 to L220, Y188 to L227 and G190 to A229 (Table 1) (27,28,47–49).

Preparation of MoMLV and XMRV RTs

The sequence coding for full-length XMRV RT from the VP-62 clone (NCBI RefSeq: NC_007815) (1) was optimized for expression in bacteria, synthesized by Epoch Biolabs and cloned as described in 'Materials and Methods' section. Both XMRV RT and MoMLV RT were tagged with a hexahistidine sequence at the N-terminus and expressed with a yield of ~2 mg/l of culture. Purified enzymes (>95% pure, Supplementary Figure S2) were stored at −20°C. The presence of NP-40 or glycerol was critical for enzyme stability.

Steady state kinetics of nucleotide incorporation

Initial polymerase activity assays using $T_{d31}/5'$-Cy3-P_{d18a} displayed overall slower polymerase activity of XMRV RT compared to HIV-1 and MoMLV RTs. This observation led us to investigate the steady state nucleotide incorporation properties of XMRV RT using single nucleotide incorporation assays. The estimated values for k_{cat} (19.9 min^{-1} for HIV-1 RT (32), 3.3 min^{-1} for MoMLV RT, 0.6 min^{-1} for XMRV RT) and $K_{m.dNTP}$ (0.07 μM for HIV-1 RT (32), 3.3 μM for MoMLV RT, 3.0 μM for XMRV RT) show that XMRV RT has a drastically reduced efficacy ($k_{cat}/K_{m.dNTP}$) at nucleotide incorporation, compared to both MoMLV and HIV-1 RTs.

DNA binding affinity

To assess if the efficiency of XMRV RT was also affected by a lower DNA binding affinity we measured the DNA binding affinity of the enzymes using three methods: gel-mobility shift assays, pre-steady state kinetics and SPR. Gel-mobility shift assays showed that the $K_{D.DNA}$ for XMRV RT was marginally higher than that for HIV-1 RT and MoMLV RT (data not shown) (50) suggesting weaker binding to DNA.

DNA binding affinity using pre-steady state kinetics

Pre-steady state kinetics allows estimation of the fraction of active polymerase sites as well as the $K_{D.DNA}$ value for the enzyme. The amplitudes of DNA extensions using XMRV RT and/or MoMLV RT at varying DNA concentrations were plotted against the DNA concentration and

Table 1. HIV-1 RT drug resistance mutations with wild-type XMRV RT and MoMLV RT residues

	HIV-1 residue numbers	HIV-1 RT wt	HIV-1 resistance mutations					XMRV RT wt	MoMLV RT wt
			3TC	ABC	TDF	D4T	EFdA		
Thymidine analog mutations (TAMs)	184	M	V	V	–	–	V	V223	V223
	41	M	–	L	L	L	–	L81	L81
	67	D	–	N	N	N	–	G105	G105
	210	L	–	W	W	W	–	N226	N226
	215	T	–	FY	FY	FY	–	A231	A231
	219	K	–			QE	–	K235	K235
Non-thymidine analog regimen mutations	65	K	RN	RN	RN	RN	–	K103	K103
	70	K	EG	EG	EG	–	–	D108	D108
	74	L	–	VI	–	–	–	V112	V112
	75	V	–	TM	M	TM	–	Q113	Q113
	115	Y	–	F	F		–	F155	F155
	69	T	Ins	Ins	Ins	Ins	–	N107	N107
Multi-NRTI resistance mutations	151	Q	M	M	M	M	–	Q190	Q190
	62	A	V	V	V	V	–	P104	P104
	75	V	–	I	–	I	–	Q113	Q113
	77	F	–	L	–	L	–	L115	L115
	116	F	–	Y	–	Y	–	F156	F156
TDRTI Mutations	184	M	V	V	–	–	V	V223	V223
	165	T	–	–	–	–	R	H204	H204

The HIV-1 RT data are based on data from the Stanford HIV Database (85).
wt = wild-type.

the data were fit to the quadratic equation (Equation 2), yielding a $K_{D.DNA}$ of 33 nM for XMRV RT, 19 nM for MoMLV RT (Table 2) and 12.5 nM for HIV-1 RT (32). These values did not change significantly when tested with DNA of different lengths (data not shown). Hence, the transient kinetic experiments confirmed the findings of the gel-mobility shift assays showing XMRV RT to have lower DNA binding affinity than HIV-1 RT.

Binding kinetics of XMRV and HIV-1 RT to double-stranded DNA

Measurements of $K_{D.DNA}$ using gel-mobility shift assays and pre-steady state kinetic methods do not offer insights regarding the kinetics of binding and release of nucleic acid from the viral polymerases. Hence, we used SPR to measure directly DNA binding and the DNA dissociation components of the $K_{D.DNA}$. We attached on the SPR chip a nucleic acid biotinylated at the 5′ template end and immobilized it on a streptavidin sensor chip. Various concentrations of either XMRV or HIV-1 RT were flowed over the chip to measure the association (k_{on}) and dissociation (k_{off}) rates of the enzymes in real time (Figure 1). HIV-1 RT had considerably slower dissociation rates than XMRV RT, and longer dissociation phases were needed to obtain reliable values.

Several methods were tested to best fit our data. The 'heterogeneous ligand' method gave the best fit for both XMRV and HIV-1 RT. In this model the x^2 values for DNA binding to XMRV and HIV-1 RT were 9.3 RU^2 and 48.1 RU^2, respectively, compared to 15.1 RU^2 and 152 RU^2 when we tried fitting the data in a 'homogeneous ligand' model. The former model assumes that RT binds DNA in two different modes and provides two association (k_{on}) and two dissociation constants (k_{off}).

Our data show that XMRV RT has a slightly faster rate of association (k_{on}) than HIV-1 RT. We measured two k_{on} values of $7.3 \times 10^6 M^{-1}s^{-1}$ and $8.2 \times 10^4 M^{-1}s^{-1}$ for XMRV RT versus $7.6 \times 10^5 M^{-1}s^{-1}$ and $1.2 \times 10^6 M^{-1}s^{-1}$ for HIV-1 RT. Interestingly, the dissociation rate of XMRV RT was significantly faster than that of HIV-1 RT ($0.28\,s^{-1}$ and $0.0045\,s^{-1}$ for XMRV RT and 7.8×10^{-4} $s^{-1}$and $0.0076\,s^{-1}$ for HIV-1 RT) (Table 3). This difference in dissociation rate resulted in a $K_{D.DNA}$ at least 1 order of magnitude higher for XMRV RT compared to HIV-1 RT (38 and 54 nM versus 1.0 and 6.1 nM for XMRV and HIV-1 RT, respectively) (Table 3).

Nucleotide binding affinity and optimal incorporation efficiency

A transient-state kinetics approach was used to estimate the dNTP binding affinity ($K_{d.dNTP}$) and maximum nucleotide incorporation rate (k_{pol}) (55). The rates at varying concentrations of next incoming nucleotide (dATP) were determined by plotting the amount of extended primer as a function of time. The rates were then plotted against dATP concentration. The data were fit to a hyperbola (Equation 3). The $K_{d.dNTP}$ for XMRV RT is 26.6 μM and the k_{pol} is $8.9\,s^{-1}$ (Figure 2) (Table 2). Under similar conditions the $K_{d.dNTP}$ and k_{pol} were 1.3 μM and $24.4\,s^{-1}$ for HIV-1 RT (29) and 25 μM and $14.1\,s^{-1}$ for MoMLV RT.

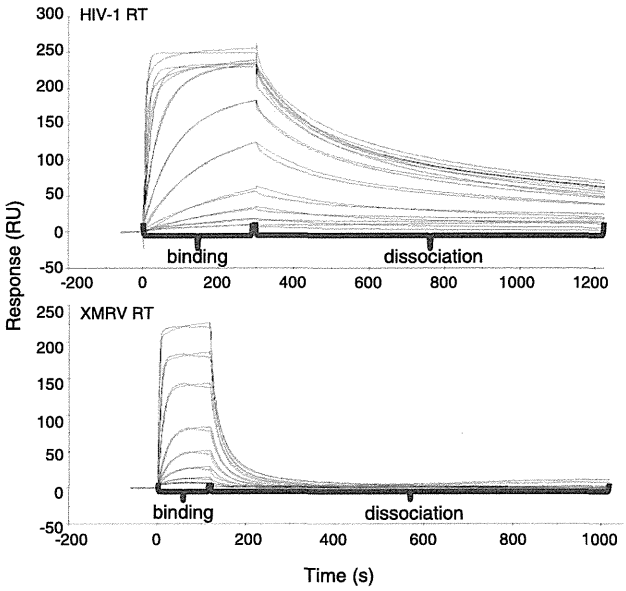

Figure 1. Assessment of $K_{D.DNA}$, k_{on} and k_{off} using surface plasmon resonance. SPR was used to measure the binding affinity of RTs to a nucleic acid substrate. Increasing concentrations of each RT (0.2, 0.5, 1, 2, 5, 10, 20, 50, 100 and 200 nM) were injected over a streptavidin chip with biotinylated double-stranded DNA immobilized on its surface as described in 'Materials and Methods' section. The experimental trace (red) shown is the result of a subtraction of the data obtained from the channel containing the immobilized nucleic acid minus the signal obtained from an empty channel. The black curve represents the fitted data according to the 'heterogeneous ligand' model that assumes two different binding modes for RT on the nucleic acid.

Table 2. Kinetic parameters of DNA binding and synthesis by HIV-1 and XMRV RTs

Nucleotide affinity and incorporation	HIV-1 RT[a]	MoMLV RT	XMRV RT
$K_{d.dNTP}$ (μM)	1.3 ± 0.4	25 ± 5.3	26.6 ± 6.5
k_{pol} (s^{-1})	24.4 ± 0.9	14.1 ± 0.8	8.9 ± 0.6
$k_{pol}/K_{d.dNTP}$ ($s^{-1}\cdot\mu M^{-1}$)	18.8	0.56	0.33
DNA binding affinity:			
$K_{D.DNA}$ (nM)	12.5	19.0	32.5

[a]HIV-1 RT data published previously (29).

Table 3. DNA binding constants for HIV-1 and XMRV RTs from surface plasmon resonance

	HIV-1 RT	XMRV RT
k_{on} ($M^{-1}.s^{-1}$)	7.6×10^5	7.3×10^6
k_{off} (s^{-1})	7.8×10^{-4}	2.8×10^{-1}
$K_{D.DNA1}$ (nM)	1	38 (38-fold)[a]
k_{on} ($M^{-1}.s^{-1}$)	1.2×10^6	8.2×10^4
k_{off} (s^{-1})	7.6×10^{-3}	4.5×10^{-3}
$K_{D.DNA2}$ (nM)	6.1	54 (9-fold)[a]

[a]Increase in $K_{D.DNA}$ (decrease in affinity) with respect to HIV-1 RT. ($K_{D1\text{-}XMRV\ RT}/K_{D1HIV\text{-}1\text{-}RT}$ and $K_{D2\text{-}XMRV\ RT}/K_{D2HIV\text{-}1\text{-}RT}$).

Fidelity of nucleotide incorporation

To assess whether XMRV RT displays high nucleotide incorporation fidelity we monitored the incorporation of three dNTPs by XMRV RT and compared with HIV-1 RT (52). The results of fidelity assay are shown in Figure 3. The lanes marked '4dNTPs' for all enzymes represent the DNA synthesis using a T_{d100}/5′-Cy3-P_{d18a} template-primer in the presence of all four dNTPs. The subsequent lanes, marked '-dNTP', correspond to the synthesis of DNA in the absence of that specific deoxynucleotide triphosphate. The comparison of the DNA synthesis in the absence of one nucleotide by HIV-1 RT, MoMLV RT and XMRV RT shows that HIV-1 and MoMLV RTs were able to misincorporate and extend the primer beyond the missing nucleotide more efficiently than XMRV RT, suggesting that the latter is a less error prone DNA polymerase. It should be noted that the higher fidelity of XMRV is not the result of measuring a smaller number of errors because of the decreased replication rate, as the assay conditions were optimized to allow production of the same amount of full length product in the presence of all four dNTPs for and MoMLV RTs. To further investigate the fidelity of DNA synthesis by XMRV RT, the kinetics of mismatch nucleotide incorporation were carried out in a quantitative manner by monitoring the incorporation of single mismatched nucleotide under pre-steady state conditions. The estimated $K_{D.dTTP}$ (mismatch) and k_{pol} values show that XMRV RT has a lower affinity for a mismatched nucleotide but comparable turnover number than MoMLV RT, suggesting that the observed higher fidelity over MoMLV RT is due to differences during the nucleotide-binding step (Table 4). However, compared to HIV-1 RT, XMRV RT has decreased both affinity and incorporation rate, suggesting that its higher fidelity is the result of both decreased binding of mismatched nucleotides and slow rate of incorporation.

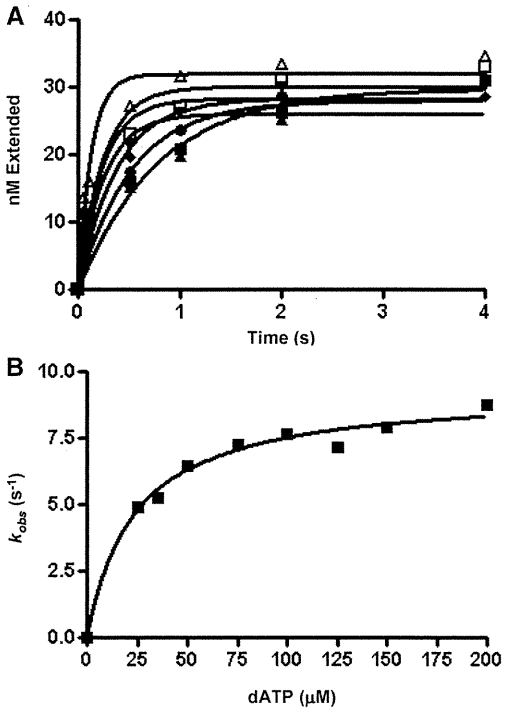

Figure 2. Pre-steady state kinetics of nucleotide incorporation by XMRV RT. 150 nM XMRV RT was pre-incubated with 40 nM T_{d31}/5′-Cy3-P_{d18a} rapidly mixed with a solution containing $MgCl_2$ (5 mM) and varying concentrations of dATP: 25 μM (filled square), 35 μM (filled triangle), 50 μM (filled inverted triangle), 75 μM (filled rhombus), 100 μM (filled circle), 125 μM (open square) and 150 μM (open triangle); and incubated for 0.1 to 6 s before being quenched with EDTA. The DNA product for each dATP concentration was fit to the burst equation (**A**). The burst amplitudes generated for each dATP concentration were then fit to a hyperbola equation (**B**) yielding the optimal rates of dNTP incorporation; k_{pol} (8.9 s^{-1}) and dNTP binding to the RT-DNA complex; $K_{d.dATP}$ (26.6 μM).

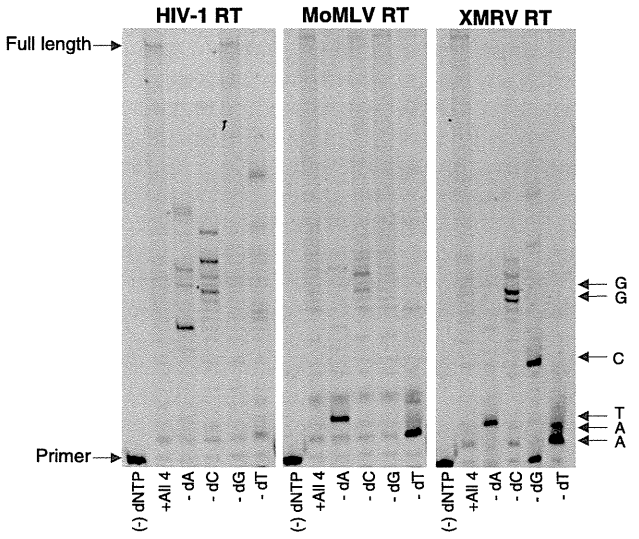

Figure 3. Comparison of *in vitro* fidelity of HIV-1, MoMLV and XMRV RTs. Extension of 10 nM T_{d100}/5′-Cy3-P_{d18a} by HIV-1 RT, MoMLV RT or XMRV RT (20, 50 and 50 nM, respectively) in the presence of 150 μM each of three out of four nucleotides (the missing nucleotide is marked at the bottom of each lane). Reactions were run for 30 min for HIV-1 RT and 45 min for XMRV RT and MoMLV RT. For each enzyme the first lane in each set shows the position of unextended primer, the second lane shows full extension in the presence of all four dNTPs, and each consecutive lane shows extension in the presence of three dNTPs. The arrows on the right mark the expected pauses based on the indicated composition of the template strand.

Table 4. Kinetics of mismatch incorporation for HIV-1, MoMLV and XMRV RTs

Enzyme	HIV-1 RT	MoMLV RT	XMRV RT
$K_{d.dNTP}$ (μM)	9 ± 0.3	38.9 ± 11.6	256 ± 72
k_{pol} (s^{-1})	6.81 ± 1.2	0.16 ± 0.01	0.15 ± 0.018
$k_{pol}/K_{d.dNTP}$ (s^{-1} • μM)	0.756	0.0041	0.00058
Fidelity[a]	0.04	0.007	0.002

[a]Fidelity is the ratio of the incorporation efficiency ($k_{pol}/K_{d.dNTP}$) of the mismatched nucleotide (dTTP) over that of the correct (dATP) ([k_{pol}/K_d]dTTP/[k_{pol}/K_d]dATP).

Intracellular fidelity by measuring LacZ mutation frequency

The ANGIE P cells used for this assay are a D17-based encapsidating cell line and contain an MLV-based retroviral vector (GA-1), which encodes a bacterial β-galactosidase gene (*lacZ*) and a neomycin phosphotransferase gene (*neo*). Replication fidelity is a measure of the frequency of *lacZ* inactivation and was determined by measuring *lacZ* non-expressing white colonies. The results show that the number of white colonies was not statistically different in the case of XMRV as compared to AM-MLV, suggesting that under these conditions the fidelity of XMRV is not significantly different than that of AM-MLV (Figure 4).

Processivity of DNA synthesis

Processivity is the probability of translocation of a polymerase along a template and predicts the number of cycles of nucleotide incorporation during one productive enzyme–DNA binding event. We assessed XMRV RT's processivity of DNA synthesis in comparison to HIV and MoMLV RTs using both a gel-based trap assay and a quantitative pre-steady state assay. In the gel-based assay, the enzymes were pre-incubated with template-primer, then the reaction was initiated by the addition of all four nucleotides together with calf thymus DNA, which was used as a trap to bind free enzyme dissociated from the substrate during the course of the reaction (38). The length of the DNA product is an inverse measure of termination probability, as previously described. As a control, we used lanes where no trap was present; establishing that the same amount of total polymerase activity (processive and non-processive) is provided in all cases. The results indicate that XMRV RT is less processive than HIV-1 and MoMLV RTs with shorter DNA product after 30 min of reaction in the presence of trap (Figure 5).

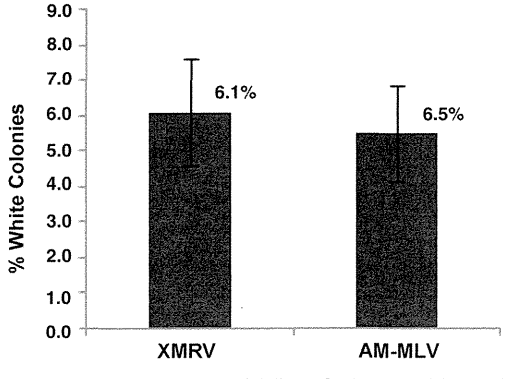

Figure 4. Comparison of *in vivo* fidelity of XMRV with amphotropic MLV. The ANGIE P cells used for this assay contain a retroviral vector (GA-1), which encodes a bacterial β-galactosidase gene (*lacZ*) and a neomycin phosphotransferase gene. Replication fidelity is measured by the frequency of *lacZ* inactivation resulting in an increase in white colonies. The fidelity differences between the two viruses are not statistically significant (error bars represent standard error from three independent experiments).

To measure processivity quantitatively we applied a single turnover processivity assay developed by Patel *et al.* (35) (Figure 6). In this assay, the rates of consecutive nucleotide incorporations under single turnover conditions are monitored. The rate of elongation incorporation (k_1) and the rate of processive DNA synthesis (k_2) (Equation 4) were calculated at several template positions for each enzyme. The ratio of the rate of processive DNA synthesis to the rate of nucleotide incorporation (k_2/k_1) is referred to as the processivity index (35). The absolute values of these constants for HIV-1 RT, XMRV and MoMLV RT and their ratios are collected in Table 5. XMRV RT is clearly the least processive for each extension product. The difference in processivity varies significantly depending on sequence or sequence context (decrease in processivity from 3-fold up to 10-fold). While the current data do not allow generalization of rules for pausing at specific sites, this clearly shows consistently that XMRV is not as efficient as MoMLV RT in polymerizing processively through 'difficult spots'.

Susceptibility of XMRV RT to NRTIs, TDRTIs and NNRTIs

Previous studies have shown that XMRV is inhibited by some antivirals (53–56). However, the susceptibility of XMRV RT has not been tested against a wide variety of

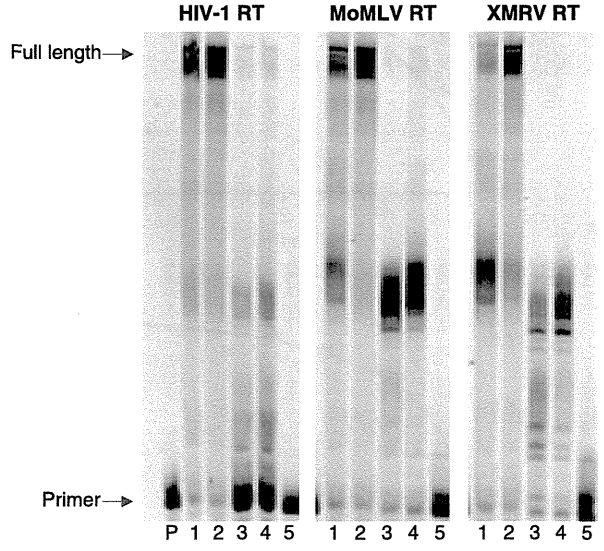

Figure 5. Processivity (trap assay) of HIV-RT, MoMLV RT and XMRV RT. DNA synthesis was monitored in the presence of calf thymus DNA as an enzyme trap. Each enzyme (30 nM HIV RT, 100 nM MoMLV RT or 100 nM XMRV RT) was pre-incubated with 40 nM T_{d100}/Cy3-P_{d18a}. Lanes 1 and 2 of each set show unlimited DNA synthesis in the absence of trap for 5 and 10 min for HIV-1 RT and 10 and 40 min for XMRV RT and MoMLV RT. In Lanes 3 and 4 the reaction is initiated by the addition of dNTPs (100 μM each) together with the calf thymus DNA trap (0.5 μg/μl) such that the products generated represent a single processive synthesis event for the respective time points for each enzyme. Lane 5 shows the effectiveness of the trap determined by incubating the calf thymus DNA with the enzyme before addition of labeled template-primer. Processive primer extension by HIV-1 RT and MoMLV RT in Lanes 4–6 of the left and middle panel is higher than by XMRV RT in Lanes 4–6 of the right panel.

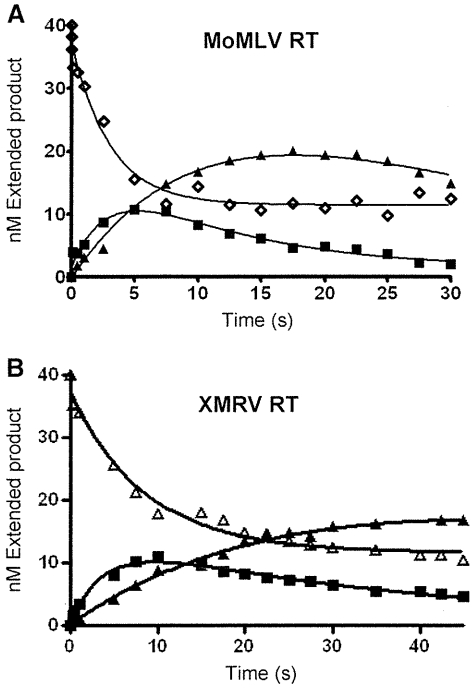

Figure 6. Single-turnover processivity assays. 30 nM T_{d31}/Cy3-P_{d18a} was combined with 100 nM XMRV RT or 50 nM MoMLV RT in RT buffer before rapidly mixing with all four dNTPs (100 μM each) and 5 mM $MgCl_2$ for varying incubation times (0.05–45 s) and quenching with EDTA. Extension of the 18-mer primer (open rhombus) ((open triangle) for XMRV RT) into 19-mer (filled square) and 22-mer (filled square), by MoMLV RT (**A**) and XMRV RT (**B**) was fit to a double exponential equation to determine rates of product appearance, and subsequent processive extension of those products (rates shown in Table 5).

Table 5. Single turnover processivity parameters of HIV-1, MoMLV and XMRV RTs

Template site	Processivity index (k_2/k_1)		
	HIV-1 RT	MoMLV RT	XMRV RT
1	6.98	0.31	0.12

1
3′-CAT TGA CAA GCT CGT GGT TAC GAT CGA TAC C
5′-Cy3-GTA ACT GTT CGA GCA CCT
The template site position monitored is underlined and labeled.

nucleoside RT inhibitors (NRTIs) that block replication by chain-terminating the primer, or by preventing translocation after their incorporation into the nascent DNA chain (TDRTIs) (32,57,58). In addition, the susceptibility of XMRV RT to non-nucleoside RT inhibitors (NNRTIs) or RNA aptamers that can be selected to block reverse transcriptases (59–63) has not been established.

Hence, we performed gel-based primer extension assays in the presence of various inhibitors. As shown in Table 6, most of the HIV-1 RT inhibitors also block XMRV RT with significantly varying IC_{50}s. The most potent inhibitors tested were ENdA (4′-ethynyl-2-amino-2′-deoxyadenosine) followed by EFdA. EFdA was also potent at

Table 6. Inhibition of XMRV and MoMLV RTs

Compound	IC_{50} (μM)	
	XMRV RT	MoMLV RT
Adefovir-DP	0.92	1.02
Tenofovir-DP	6.4	1.51
D4T-TP	0.77	2.37
3TC-TP	21	10
EFdA-TP	0.43	0.29
ENdA-TP	0.14	0.18

D4T, stavudine or 2′,3′-dehydro-2′,3′-deoxythymidine; 3TC, lamivudine; EFdA, 4′-ethynyl-2-fluoro-2′-deoxyadenosine; ENdA, 4′-ethynyl-2-amino-2′-deoxyadenosine.

inhibiting wild-type XMRV replication in cell culture with an EC_{50} of 40 nM from three independent experiments (standard error was 10 nM).

Unlike HIV-1 RT, XMRV RT and MoMLV RT lack the two tyrosine residues (Y181 andY188 in HIV-1 RT) (Supplementary Figure S1) that are known to contribute to NNRTI binding. Hence, the gammaretroviral enzymes were not inhibited by the NNRTIs tested (TMC-125 and efavirenz) (Supplementary Figure S3).

Susceptibility of XMRV RT to RNA aptamers

We also tested XMRV RT's susceptibility to three independent RNA aptamers that had been previously selected against MoMLV RT (60). The aptamers inhibited XMRV RT to varying extents with IC_{50}s ranging from 2 to 52 nM (Figure 7). Most notable was the m.1.1FL aptamer which gave IC_{50}s of 2 and 4 nM for XMRV RT (Figure 7) and MoMLV RT respectively, without inhibiting HIV-1 RT (data not shown). These inhibition assays utilized truncated forms of aptamers m.1.3 and m.1.4 lacking the original primer-binding segments of the aptamers, demonstrating that these 5′ and 3′ segments are not required.

PPi-mediated excision activity of XMRV RT

A key mechanism of NRTI resistance in HIV-1 RT is based on inhibitor excision from the primer end, using a pyrophospholytic reaction (64,65). The pyrophosphate donor *in vivo* is likely to be ATP, although PPi can efficiently unblock NRTI-terminated primers. This excision activity is present in wild-type HIV-1 RT, and is enhanced in the presence of AZT-resistance mutations. We measured the ability of wild-type XMRV to unblock primers terminated with AZT or EFdA in the presence of PPi. We found that unlike HIV-1 RT that excised AZT-MP efficiently under these conditions, XMRV RT had considerably lower excision activity (Figure 8). Similar excision experiments where ATP was used instead of PPi showed that XMRV is very inefficient in ATP-based excision as compared to HIV-1 RT (data not shown).

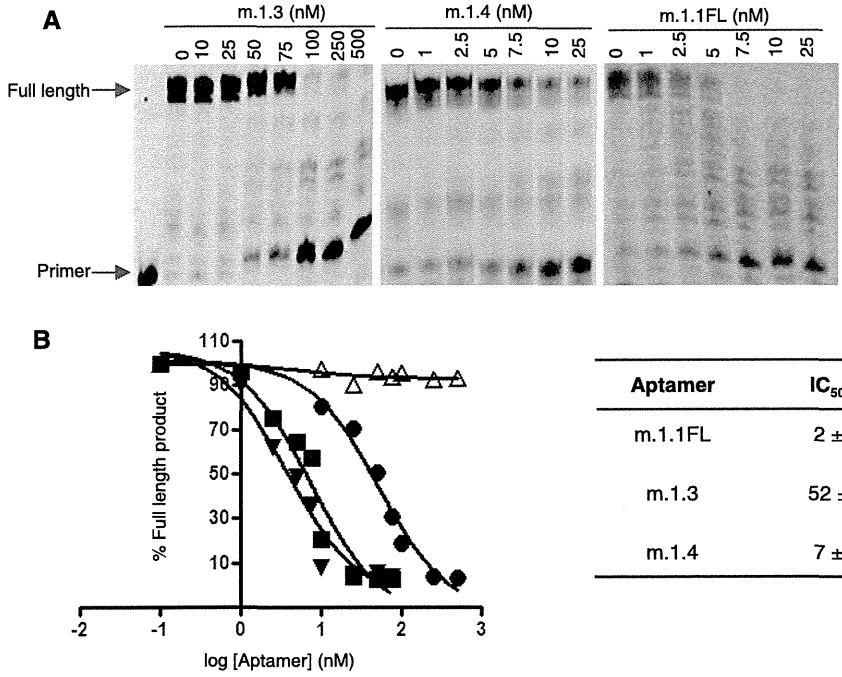

Aptamer	IC_{50} (nM)
m.1.1FL	2 ± 0.15
m.1.3	52 ± 0.27
m.1.4	7 ± 0.16

Figure 7. Inhibition of XMRV RT by RNA aptamers. 10 nM XMRV RT was incubated with increasing amounts of RNA aptamer in Reaction Buffer for 5 min at 37°C followed by addition of 20 nM T_{d31}/Cy3-P_{d18a} and 50 μM of each dNTP. (**A**) The reactions were stopped after 30 min and resolved on a polyacrylamide gel. The predicted secondary structures of each aptamer were generated by mfold. (**B**) The percent full extension was quantified for m.1.1FL (filled inverted triangle), m.1.3 (filled circle) and m.1.4 (filled square) and data points fit to one-site competition non-linear regression using GraphPad Prism 4 to calculate IC_{50}. HIV-1 RT was not susceptible to m.1.1FL (open triangle). (Errors represent data deviation from the fit).

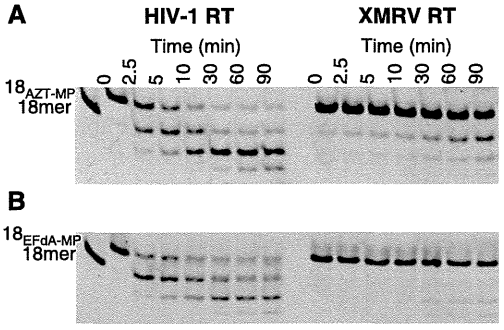

Figure 8. PPi-mediated unblocking of AZT-(A) and EFdA-(B) terminated DNA. About 20 nM of (**A**) AZT- or (**B**) EFdA-terminated T_{d31}/Cy3-P_{d18c} ($T/P_{AZT\text{-}MP}$ or $T/P_{EFdA\text{-}MP}$) was incubated with HIV-1 RT (60 nM) or XMRV RT (200 nM) in the presence of 150 μM PPi and 6 mM $MgCl_2$. Aliquots of the reactions were stopped at different time points (0–90 min) and resolved on a 15% polyacrylamide–7M urea gel as described in the 'Materials and Methods' section.

Susceptibility of mutant XMRV RTs to AZT-TP and tenofovir-DP

The HIV-1 RT mutation Q151M confers resistance to AZT by enhancing discrimination of the nucleotide analog leading to its reduced incorporation (37,66–68). Another HIV-1 RT mutation, K65R, decreases susceptibility to tenofovir (69,70). Since AZT and tenofovir are potent inhibitors of XMRV (Table 6) (54–56), we wanted to investigate whether the XMRV RT mutant equivalents of HIV Q151M and K65R (XMRV Q190M and K103R) would confer XMRV RT resistance to AZT and tenofovir. We constructed these mutant clones and tested their susceptibility to AZT and tenofovir in the same manner as wild-type XMRV RT. Interestingly, Q190M XMRV RT has a decreased susceptibility to AZT (approximately 5-fold increase in the IC_{50}). Similarly, the K103R XMRV RT mutant enzyme was less susceptible to tenofovir, increasing the IC_{50} by at least 2-fold.

Molecular model of XMRV RT

Given the significant sequence similarity between XMRV and MoMLV RTs, the resulting homology model of XMRV RT is highly similar to MoMLV RT (>1.5Å rms) and of excellent quality. Since the input structure of MoMLV RT did not contain the RNase H domain of the enzyme, the XMRV RT model is also missing this domain. The molecular model of the polymerase domain of XMRV RT is shown in Figure 9. An alignment of the MoMLV RT crystal structure (22) with the XMRV RT homology model highlights the few changes in the polymerase domain of XMRV RT. These are L29 (P in MoMLV), Q234 (L in MoMLV), R238 (Q in MoMLV) and N422 (D in MoMLV). From these, residue 422 is located in the nucleic acid binding cleft and may contribute to differences in the interactions with nucleic acid substrate. However, most of the differences between the gammaretroviral enzymes are in their RNase H domains and also in the first 30 N-terminal residues of the polymerase domain, for which we do not have structural